

# Multiple change-point detection for some point processes

Charlotte Dion-Blanc<sup>(1)</sup>, Diala Hawat<sup>(1+)</sup>, Émilie Lebarbier<sup>(2)</sup>, Stéphane Robin<sup>(1)</sup>,  
(1) LPSM, Sorbonne Université, CNRS, Paris 75005, France  
(2) Modal'X, Université Paris Nanterre, CNRS, UPL, Nanterre, 92000, France

## Abstract

The aim of change-point detection is to identify behavioral shifts within time series data. This article focuses on scenarios where the data is derived from an inhomogeneous Poisson process or a marked Poisson process. We present a methodology for detecting multiple offline change-points using a minimum contrast estimator. Specifically, we address how to manage the continuous nature of the process given the available discrete observations. Additionally, we select the appropriate number of changes via a cross-validation procedure which is particularly effective given the characteristics of the Poisson process. Lastly, we show how to use this methodology to self-exciting processes with changes in the intensity. Through experiments, with both simulated and real datasets, we showcase the advantages of the proposed method, which has been implemented in the R package `CptPointProcess`.

*Keywords:* Change-point detection, Point process, Dynamic programming, Exact optimization, Cross-Validation

## 1 Introduction

Detecting multiple change-points is one of the most common tasks in statistics, data analysis and signal processing. The problem can be formulated as follows: considering a process observed over time, identify the time instants, called change-points, before and after which the intensity of the process is different. Here, we consider the detection of change-points in the distribution of a point process. More precisely, we consider a heterogeneous Poisson process, assuming that its intensity function is piecewise constant, and seek to find the times when the intensity value changes.

### 1.1 State of the art

**Change-point detection.** Change-point detection has been widely studied in the literature (see e.g. Niu et al., 2016; Truong et al., 2020, for surveys). Existing methods can be organized according to a few main alternatives: (a) single or multiple change-point detection, (b) online or offline configuration, (c) frequentist or Bayesian statistical inference, (d) discrete or continuous time; all combinations have been considered in one way or another. Single change-point detection focuses on the existence of a single change, while multiple-point detection takes into account a series of changes. The online framework aims to detect changes while the process is being observed, while the offline framework addresses the problem of detection once the process has been observed for a given period of time. We consider here the problem of detecting multiple change-points in the offline framework, for which we adopt a frequentist approach. An important specificity of our work is that we deal with a continuous point process.

**Poisson process and Hawkes processes.** Here we consider Poisson processes (see Andersen et al., 1993; Daley and Vere-Jones, 2007, for a general introduction), which have been used as reference models in a wide range of fields, including vulcanology (Bebbington, 2007), epidemiology (Shmueli and Burkom, 2010; Tsui et al., 2008) or even cyber-attack modeling (Bessy-Roland et al., 2021; El Karoui et al., 2017). Readers can refer to Li et al. (2017b) for online detection of changes in a Poisson process. For the same process, Bayesian approaches have been proposed by Raftery and Akman (1986) or Gupta and Baker (2015) for the detection of a single change-point and by Young Yang and Kuo (2001) or Shaochuan (2021) for the detection of multiple change-points. As already mentioned, we place our work within the framework of multiple, off-line frequentist detection, just like Fromont et al. (2023), which uses multiple testing techniques, whereas we adopt a segmentation point of view. The present article allows also to deal with a self-exciting process, which is a modified Hawkes process with change-points. Only few references allow to tackle the Hawkes process, and most of them are online-procedures as Li et al. (2017a); Wang et al. (2023).

**Statistical issues.** From a statistical point of view, change-point detection raises three main problems: (i) locating the change-points, (ii) estimating the parameters governing the process between change-points and (iii) estimating the number of change-points. Problem (ii) is generally not difficult to handle using, for example, maximum likelihood, once the change-points have been identified (see e.g. Young Yang and Kuo, 2001). Determining the number of change-points (iii) is a typical model selection problem, which is examined later. Determining the position of change-points (i) is a more complex problem, mainly because it involves minimizing contrast (e.g. negative log-likelihood), which is not a continuous function of the change-point locations.

**Minimizing a non-continuous contrast.** It is known that offline detection of multiple change-points in discrete time raises a specific optimization problem for determining the optimal locations of change-points (i.e. the set of locations that minimize a given contrast), since classical contrasts, such as least-squares or negative log-likelihood, are not continuous with respect to the change-points because the locations of change-points are themselves discrete (see for example Bai and Perron, 2003; Lebarbier, 2005). Consequently, the so-called segmentation space (i.e. the – enormous, albeit finite– set of possible change-point locations) must be explored in some way. However, for a given number of segments and provided the contrast is additive with respect to the segments, this can be achieved using dynamic programming (DP) (Auger and Lawrence, 1989), with quadratic complexity.

The optimization problem may seem simpler for point processes with continuous-time change points, but it turns out to be even more complex because, as we'll show, most classical contrasts are still not continuous functions of the change points and the segmentation space is now infinite. This latter problem can obviously be circumvented by discretizing time (see Achcar et al., 2008, for medicine), (see Achcar et al., 2011, for pollution monitoring), and (see Shen and Zhang, 2012, for genomics), at the price of computational efficiency and/or accuracy. Exploration of the continuous segmentation space has been considered by West and Ogden (1997) or Young Yang and Kuo (2001) to detect a single change-point in a Poisson process. Importantly, Young Yang and Kuo (2001) observes that the negative log-likelihood is in fact concave between two successive event times, allowing the problem to be solved in a simple and exact manner. This observation is in fact essential and paves the way for the strategy we propose here for the detection of multiple change-points.

For a piecewise Hawkes process, in the specific case of maximum likelihood inference, the segment-additivity condition required by DP is clearly not satisfied except in the case where the memory of the process is lost at every change-point. But the latter case is not really realistic for many applications. To circumvent the algorithmic problem, the key idea is to use time-scaling theorem, from Papangelou (1972), to transform the process back into a Poisson process.

## 1.2 Our contribution

In this paper, we propose an efficient method for segmenting a heterogeneous Poisson process. A key aspect of our work is to show that, under reasonable assumptions regarding the contrast, the optimal segmentation can be found within a known finite grid, allowing for recovery through dynamic programming. A crucial assumption is that the contrast is additive with respect to the segment, which stems from the inherent properties of Poisson processes. We also examine admissible contrasts, in the sense that they do not produce undesirable solutions. For determining the number of segments, we employ a cross-validation approach inspired by Arlot and Celisse (2011). A notable feature of this procedure is its validity, which arises from the thinning property of Poisson processes. Furthermore, our methodology can be extended to the segmentation of marked Poisson processes.

The proposed method has been implemented in the R package `CptPointProcess`, which is available at [github.com/Elebarbier/CptPointProcess](https://github.com/Elebarbier/CptPointProcess).

Eventually, we consider the extension of the proposed procedure to a piecewise Hawkes process. More specifically, based on a prior estimate of the compensator of the observed process, we show to transform it back to an heterogeneous Poisson process to which our methodology applies.

**Outline.** We present the model in Section 2. Next, the optimization procedure for a given number of segments is described in Section 3 and the admissible contrasts are discussed in Section 4. This methodology is first extended to marked Poisson processes in Section 5 and to Hawkes(-like) processes in Section 6. Section 7 presents the proposed procedure for selecting the number of segments. Numerical experiments on synthetic data are presented in Section 8 and the use of the whole methodology is illustrated on earth science datasets in Section 9. Some elements of proofs are given in Section 11.

## 2 Poisson model

Consider a general Poisson process  $\{N_t\}_{0 \leq t \leq 1}$  with intensity  $t \mapsto \lambda(t)$  and denote  $N_t = N((0, t])$  the number of events occurring over the interval  $[0, t]$ . Let's denote  $T_1, \dots, T_{N_1}$  the event times observed over the observation time interval  $[0, 1]$ , such that  $N_{T_i} - N_{T_i^-} = 1$  with the convention  $T_0 = 0$  and  $T_{N_1+1} = 1$ . We assume that  $T_j - T_j^- = 0$  for all  $j$  and designate  $N_1 = n$  for simplicity. In the following, we work conditionally on this event.

We assume that the intensity of the process is piecewise constant. Let  $m$  be a partition of  $[0, 1]$  composed of  $K$  segments denoted  $I_k := (\tau_{k-1}, \tau_k]$  for  $k = 1, \dots, K$  where  $0 = \tau_0 < \tau_1 < \dots < \tau_K = 1$  are called the change-points, and  $\boldsymbol{\tau} = (\tau_1, \tau_2, \dots, \tau_{K-1})$  the vector of  $K - 1$  unknown change-points. Thus, the partition  $m$  is defined as  $m := \{I_k\}_{1 \leq k \leq K}$  and the associated intensity of the process is

$$\lambda(t) := \sum_{k=1}^K \lambda_k \mathbb{1}_{I_k}(t), \quad (1)$$

where  $\lambda_k$  is the intensity in segment  $I_k$ . The vector of intensities is denoted  $\boldsymbol{\lambda} = (\lambda_1, \lambda_2, \dots, \lambda_K)$ . This model corresponds to a piecewise homogeneous Poisson process: we call it the change-point Poisson model.

Let  $\Delta\tau_k := \tau_k - \tau_{k-1}$  be the length of the interval  $I_k$  and  $\Delta N_k := N((\tau_{k-1}, \tau_k]) = N(\tau_k) - N(\tau_{k-1})$  the number of events occurring in the interval  $I_k$ . The probability of a given path  $\{N_t\}_{0 \leq t \leq 1}$  (which we denote by  $N$ ) for the Poisson change-point model (identified by a subscript  $P$ ) is then as follows

$$p_P(N; \boldsymbol{\tau}, \boldsymbol{\lambda}) = \prod_{k=1}^K e^{-\lambda_k \Delta\tau_k} \lambda_k^{\Delta N_k}. \quad (2)$$

We can easily see that, for a given  $\tau$ ,  $p_P(N; \tau, \lambda)$  is maximal for  $\hat{\lambda}_k(\tau) = \Delta N_k / \Delta \tau_k$ ,  $1 \leq k \leq K$ . Consequently, the objective is to find the set of maximum-likelihood change-point locations that minimize the Poisson contrast:

$$\gamma_P(\tau; N) := -\log p_P(N; \tau, \hat{\lambda}(\tau)) = \sum_{k=1}^K \Delta N_k \left( 1 - \log \left( \frac{\Delta N_k}{\Delta \tau_k} \right) \right). \quad (3)$$

Note that  $\gamma_P$  is additive with respect to segments, due to the independence of the event times in disjoint segments: this property plays an essential role in the sequel.

### 3 Optimal change-points

We now consider the determination of the optimal set of change-point locations  $\hat{\tau}$ , defined as the minimizer of a given data-dependent contrast  $\gamma(\tau; N)$ , such as the Poisson contrast  $\gamma_P$  defined in (3). An important feature of the resulting optimization problem on  $(0, 1)^{K-1}$  is that the function  $\gamma$  may not be convex, or even continuous with respect to  $\tau_k$  (the Poisson contrast  $\gamma_P$  is neither). Consequently, classical optimization strategies such as gradient descent do not apply.

Still in the context of single change-point detection, Young Yang and Kuo (2001) makes the critical observation that the Poisson contrast  $\gamma_P$  is in fact concave on every inter-event interval  $[T_i, T_{i+1}[$ , so that the optimal change-point is necessarily located at an event time  $T_i$  or just before, in  $T_i^-$ . Extending Young Yang and Kuo (2001), we show that, in the context of multiple change-point detection with a given number of segments  $K$ , some assumptions on the contrast function are sufficient to guarantee that the optimal change-points  $\hat{\tau}_k$  ( $1 \leq k \leq K-1$ ) are all located at, or just before, an event time. This observation reduces the original continuous-space optimization problem to a discrete-space optimization problem, for which efficient and exact algorithms exist.

#### 3.1 Segmentation space and partitioning

For a fixed number of segments  $K$ , we define the segmentation space as the set of all possible partitions of  $(0, 1)$  into  $K$  segments:

$$\mathcal{M}^K := \{ \tau = (\tau_1, \dots, \tau_{K-1}) \in (0, 1)^{K-1}; 0 = \tau_0 < \tau_1 < \dots < \tau_K = 1 \}.$$

An element of  $\mathcal{M}^K$  (i.e. a "segmentation") is therefore a sequence of change-points. In addition, we define the set of all possible  $K$ -uplets of integers, possibly null, whose sum is  $n$ :

$$\Upsilon^{K,n} := \left\{ \nu := (\nu_1, \dots, \nu_K) \in \{0, 1, \dots, n\}^K, \sum_{k=1}^K \nu_k = n \right\}. \quad (4)$$

It's a finite set with cardinality  $|\Upsilon^{K,n}| = \binom{n+K-1}{K-1}$ . Then, for a fixed  $\nu \in \Upsilon^{K,n}$  and a given path  $N = \{N_t\}_{0 \leq t \leq 1}$  with  $n$  events (i.e.  $N_1 = n$ ), we define the subset of segmentations from  $\mathcal{M}^K$  with a prescribed number of events in each segment given by  $\nu$ , as follows

$$\mathcal{M}_\nu^K(N) := \{ \tau \in \mathcal{M}^K, \forall 1 \leq k \leq K : \Delta N_k = \nu_k \}. \quad (5)$$

It's important to note that this constraint is equivalent to imposing that, for each  $1 \leq k \leq K-1$ ,

$$\tau_k \in \left[ T_{\sum_{j=1}^k \nu_j}, T_{\sum_{j=1}^k \nu_j + 1} \right)$$

by setting  $T_0 = 0$  and  $T_{n+1} = 1$ . It is obvious that the count vectors  $\nu \in \Upsilon^{K,n}$  induce a partition of the segmentation space  $\mathcal{M}^K$ :

$$\mathcal{M}^K = \bigcup_{\nu \in \Upsilon^{K,n}} \mathcal{M}_\nu^K(N), \quad \{\nu \neq \nu'\} \Rightarrow \{\mathcal{M}_\nu^K(N) \cap \mathcal{M}_{\nu'}^K(N) = \emptyset\}.$$

Figure 1 shows the segmentation space  $\mathcal{M}^K$  for  $K = 3$  and its partition into all subsets  $\mathcal{M}_\nu^K(N)$  for  $\nu \in \Upsilon^{K,n}$  with  $n = 4$  events. The gray region labeled by  $\nu = (2, 1, 1)$  is  $\mathcal{M}_\nu^K(N)$ , i.e., the set of all segmentations in  $(0, 1)^2$  such that  $\Delta N_1 = 2, \Delta N_2 = 1, \Delta N_3 = 1$  or, equivalently,  $T_2 \leq \tau_1 < T_3$  and  $T_3 \leq \tau_2 < T_4$ .

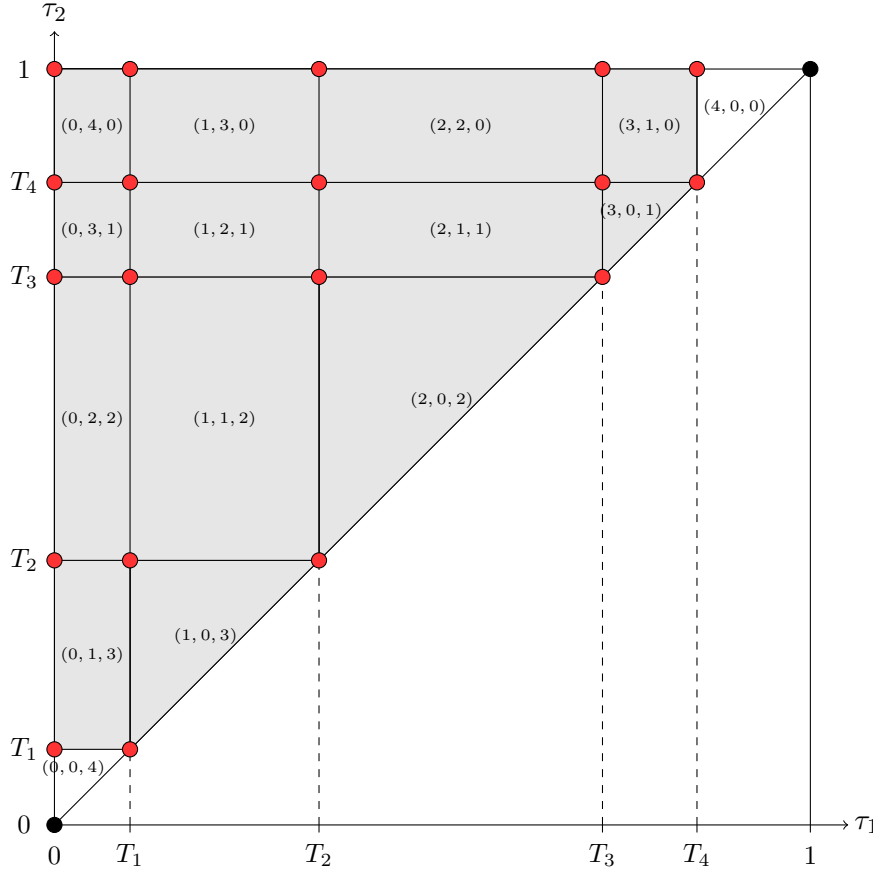


Figure 1: Segmentation space  $\mathcal{M}_\star^K$  for  $K = 3$  and  $N_1 = n = 4$  in gray. Each gray block in the upper triangle corresponds to an element of  $\Upsilon_\star^{K,n}$ . Each white block in the upper triangle corresponds to an element of  $\Upsilon^{K,n} \setminus \Upsilon_\star^{K,n}$ .

For obvious reasons, we do not consider the configurations  $\nu$  that may contain more than two successive zeros, i.e. one of the interval  $[T_{\sum_{j=1}^k \nu_j}, T_{\sum_{j=1}^k \nu_j + 1})$  contains more than two changes. This may occur only when  $K > 2$ . We therefore restrict the segmentation space to

$$\mathcal{M}_\star^K := \bigcup_{\nu \in \Upsilon_\star^{K,n}} \mathcal{M}_\nu^K(N), \quad (6)$$

where

$$\Upsilon_\star^{K,n} = \{\nu \in \Upsilon^{K,n}, \text{ for } 2 \leq k \leq K-1: \text{ if } \nu_k = 0 \text{ then } \nu_{k-1} \neq 0 \text{ and } \nu_{k+1} \neq 0\} \quad (7)$$

is of cardinality

$$|\Upsilon_{\star}^{K,n}| = \sum_{h=1}^K \binom{n-1}{h-1} \binom{h+1}{K-h},$$

with the convention  $\binom{p}{q} = 0$  if  $q > p$ . In Figure 1, the forbidden segmentation subsets (i.e. the elements of  $\Upsilon^{K,n} \setminus \Upsilon_{\star}^{K,n}$ ) are the white upper triangular regions labeled with  $\nu = (0, 0, 4)$  and  $\nu = (4, 0, 0)$ , respectively.

### 3.2 Minimum contrast estimation

We are now looking for the optimal segmentation (i.e. the sequence of change-points)  $\hat{\tau}$  with  $K$  segments that minimizes a given contrast  $\gamma$  within  $\mathcal{M}_{\star}^K$ :

$$\hat{\tau} = \operatorname{argmin}_{\tau \in \mathcal{M}_{\star}^K} \gamma(\tau). \quad (8)$$

As the number of segments  $K$  is constant in the rest of the section, the exponent  $K$  can be omitted for clarity.

The methodology we propose is based on two main assumptions on the contrast function  $\gamma$ .

**Assumption 3.1** (Segment-additivity assumption). *For each  $\nu \in \Upsilon_{\star}^n$  and for all  $\tau \in \mathcal{M}_{\nu}(N)$ , the contrast  $\gamma$  writes as sum of segment-specific cost functions:*

$$\gamma(\tau) = \sum_{k=1}^K C(\nu_k, \Delta\tau_k).$$

As an example, for the Poisson contrast  $\gamma_P$  defined in (3), the cost function is  $C(\nu_k, \Delta\tau_k) = \nu_k (1 - \log(\nu_k / \Delta\tau_k))$ .

**Assumption 3.2** (Concavity assumption). *For each  $\nu \in \Upsilon_{\star}^n$  and each  $1 \leq k \leq K$ , the cost function  $C(\nu_k, \Delta\tau_k)$  is a concave function of  $\Delta\tau_k$ .*

Under Assumption 3.1, by partitioning the segmentation space, the optimization problem (8) can be rewritten as follows

$$\hat{\tau} = \operatorname{argmin}_{\nu \in \Upsilon_{\star}^{K,n}} \min_{\tau \in \mathcal{M}_{\nu}^K(N)} \gamma(\tau) = \operatorname{argmin}_{\nu \in \Upsilon_{\star}^{K,n}} \min_{\tau \in \mathcal{M}_{\nu}^K(N)} \sum_{k=1}^K C(\nu_k, \Delta\tau_k). \quad (9)$$

We now show that the concavity assumption 3.2 for each cost function  $C$  implies piecewise concavity of the contrast  $\gamma$  with respect to  $\tau$ .

**Proposition 3.3.** *Under Assumption 3.2, for each  $\nu \in \Upsilon_{\star}^{K,n}$ , the contrast function  $\tau \rightarrow \gamma(\tau)$  is concave with respect to the segmentation  $\tau$  within  $\mathcal{M}_{\nu}^K(N)$ .*

### 3.3 Exact optimization

We now show that the optimal segmentation necessarily belongs to a finite subset of  $\mathcal{M}_\star^K$ . More precisely, it necessarily belongs to a finite and known grid, so that the optimal solution can be obtained in an exact and fast manner.

**Theorem 3.4.** *Under Assumptions 3.1 and 3.2, for a fixed  $\nu \in \Upsilon_\star^{K,n}$  we get*

$$\hat{\tau} = \underset{\tau \in \mathcal{M}_\nu^K(N)}{\operatorname{argmin}} \gamma(\tau) \in \{T_{\nu_1}, T_{\nu_1+1}^-\} \times \{T_{\nu_1+\nu_2}, T_{\nu_1+\nu_2+1}^-\} \times \dots \times \{T_{\nu_1+\dots+\nu_K}, T_{\nu_1+\dots+\nu_K+1}^-\}.$$

*Proof.* The proof follows directly from the concavity of the contrast function  $\gamma(\tau)$  with respect to  $\tau \in \mathcal{M}_\nu^K(N)$  (see Proposition 3.3).  $\square$

Theorem 3.4 guarantees that the  $K - 1$  optimal change-points in each subset of  $\mathcal{M}_\nu^K(N)$  is necessarily one of its boundary partitions, thus reducing the search to a finite set of possible solutions. These solutions are illustrated in Figure 1 by the red circles for the simple case of  $K = 3$  segments (or 2 change-points). For example, for  $\nu = (2, 1, 1)$ ,  $T_2 \leq \tau_1 < T_3$  and  $T_3 \leq \tau_2 < T_4$  leading to four possible choices for the optimal solution:  $(\hat{\tau}_1, \hat{\tau}_2) = (T_2, T_3), (T_2, T_4^-), (T_3^-, T_3)$  or  $(T_3^-, T_4^-)$ .

Consequently, the optimal change-points in  $\mathcal{M}_\star^K$  are necessarily located at or just before an event  $T_i$ , in  $T_i^-$ . Moreover, for obvious reasons, for  $K > 2$ , the configuration  $(\nu_k, \Delta\tau_k) = (0, 0)$  is not taken into account. This configuration corresponds to cases where  $\tau_{k-1}$  and  $\tau_k$  belong to the same inter-event interval  $\left[ T_{\sum_{j=1}^{k-1} \nu_j}, T_{\sum_{j=1}^{k-1} \nu_j+1} \right)$  and  $\tau_{k-1} = \tau_k$ . The global optimization problem is thus reduced to a discrete optimization problem on the finite grid

$$\mathbf{tp} = \{T_1^-, T_1, T_2^-, T_2, \dots, T_n^-, T_n\},$$

with cardinal  $2n$ . This problem is well known in the context of discrete change-point detection and can be solved using the classical dynamic programming (DP) algorithm. This algorithm and its principle are presented in Appendix B in a general context of discrete time detection and we then explain how to apply it on a fixed grid. In our case, the number of points of the grid is  $2n$  so the complexity algorithm is  $\mathcal{O}(n^2K)$ . This algorithm can be used here thanks to the segment-additivity Assumption 3.1 of the  $\gamma$  contrast function.

## 4 Proposed admissible contrasts

In this section, we present two admissible contrasts in the sense that they satisfy the two Assumptions 3.1 and 3.2 and discuss the relevance of their optimal solutions.

First let consider the classical negative log-likelihood Poisson contrast which is written, for a given  $N$  path of the Poisson change-point model, a fixed  $\nu \in \Upsilon_\star^{K,n}$  and any  $\tau \in \mathcal{P}_\nu^K(N)$ , as follows

$$\gamma_P(\tau) = -\log p_P(N; \tau, \hat{\lambda}) = \sum_{k=1}^K \nu_k \left( 1 - \log \left( \frac{\nu_k}{\Delta\tau_k} \right) \right) = \sum_{k=1}^K C(\nu_k, \Delta\tau_k). \quad (10)$$

The independence property between the disjoint time-intervals of the Poisson process guarantees that the additivity Assumption of the segments 3.1 is true. It is then easy to see that the cost function  $C$  is concave with respect to  $\Delta\tau_k$ , and that Assumption 3.2 is valid.

However, this contrast, as the one based on least-squares, see Appendix A, inevitably leads to an optimal solution for  $K > 2$  that contains zero-length segments. The reason is easy to understand: the

cost  $C(1, 0) = -\infty$ . For obvious reasons, such solutions are undesirable.

We therefore propose another admissible based-likelihood contrast which does not have the same drawback. To do this, we adopt a Bayesian approach and assume that the intensities  $\lambda_k$  are independent random variables and follow a Gamma distribution with parameters  $a > 0$  and  $b > 0$ . For a fixed  $\nu \in \Upsilon_{\star}^{K,n}$  and all  $\tau \in \mathcal{P}_{\nu}^K(N)$ , the proposed contrast, the so-called Poisson-Gamma contrast, is

$$\begin{aligned} \gamma_{PG}(\tau) &= -\log p_{PG}(N; \tau; a, b) = -\log \int p_{PG}(N, \lambda; \tau, a, b) d\lambda, \\ &= \sum_{k=1}^K \left( -a \log b + \log \Gamma(a) + \tilde{a}_k \log \tilde{b}_k - \log \Gamma(\tilde{a}_k) \right) = \sum_{k=1}^K C(\nu_k, \Delta\tau_k), \end{aligned} \quad (11)$$

where  $\tilde{a}_k = \nu_k + a$ ,  $\tilde{b}_k = \Delta\tau_k + b$ . The details of the derivation of this contrast are given in Appendix A. This contrast also satisfies Assumptions 3.1 and 3.2 and is therefore admissible. In addition,  $C(1, \Delta\tau_k)$  is now lower-bounded, allowing another segmentation to be preferred to the undesirable previous ones.

Note that  $a$  and  $b$  must be chosen in practice. Since the mean of the Gamma distribution with parameters  $(a, b)$  is  $a/b$ , a simple rule is to choose  $a$  and  $b$  so that  $a/b = n$ .

Moreover, the conditional distribution of  $(\lambda \mid N; \tau)$  is a Gamma distribution with parameters  $\tilde{a}_k$  and  $\tilde{b}_k$ , thus its posterior mean is

$$\mathbb{E}(\lambda_k \mid N, \tau) = \tilde{a}_k / \tilde{b}_k. \quad (12)$$

We thus obtain the estimator  $\hat{\lambda}_k = \tilde{a}_k / \tilde{b}_k$  and we can construct the estimator of the intensity process  $(\lambda(t))_{t \in [0,1]}$ . We will use this estimator in the final algorithm (see Section 7).

## 5 Extension to marked Poisson process

We extend the proposed methodology to a marked Poisson process for which both the intensity function of the underlying Poisson process and the parameter of the distribution of the marks are affected by the same changes.

### 5.1 Model

Let us consider a marked Poisson process. More specifically, we consider a Poisson process  $N$  with a piecewise constant intensity function  $\lambda$  given in Equation (1) and suppose that a mark  $X_i$  is associated with each event time  $T_i$  ( $1 \leq i \leq n = N_1$ ).

We assume that the marks  $\{X_i\}_{i=1,\dots,n}$  are independent exponential random variables with parameter  $\rho(T_i)$ :  $X_i | T_i \sim \mathcal{E}(\rho(T_i))$ . The function  $\rho$  is assumed to be piecewise constant with the same change-points as  $\lambda$ , for  $t \in [0, 1]$ :

$$\rho(t) = \sum_{k=1}^K \rho_k \mathbb{1}_{I_k}(t), \quad \rho = (\rho_1, \dots, \rho_K). \quad (13)$$

We take the exponential distribution as an example: this setting work can easily be extended to other distributions for the marks.



## 5.2 Admissible contrasts

The log-likelihood of a given marked Poisson path  $(N, X)$  with piecewise intensity and piecewise marks distribution, is given by

$$\log p_{MP}(N, X; \boldsymbol{\tau}, \boldsymbol{\lambda}, \boldsymbol{\rho}) = \sum_{k=1}^K \left( \Delta N_k \log(\lambda_k) - \lambda_k \Delta \tau_k + \sum_{i, T_i \in I_k} \log(p(X_i | T_i; \rho_k)) \right).$$

It can be easily seen that, for a given  $\boldsymbol{\tau}$ ,  $\log p_{MP}(N, X; \boldsymbol{\tau}, \boldsymbol{\lambda}, \boldsymbol{\rho})$  is maximal for  $\hat{\lambda}_k(\boldsymbol{\tau}) = \Delta N_k / \Delta \tau_k$  and

$$\hat{\rho}_k(\boldsymbol{\tau}) = \frac{\Delta N_k}{S_k}, \quad \text{with } S_k = \sum_{i, T_i \in I_k} X_i,$$

for  $1 \leq k \leq K$ . The resulting contrast function for the estimation of the change-points is thus writes for a fixed  $\boldsymbol{\nu} \in \Upsilon_*^{K, n}$  and for all  $\boldsymbol{\tau} \in \mathcal{P}_\nu^K(N)$  as

$$\gamma_{MP}(\boldsymbol{\tau}) = -\log p_{MP}(N, X; \boldsymbol{\tau}, \hat{\boldsymbol{\lambda}}, \hat{\boldsymbol{\rho}}) = \sum_{k=1}^K \nu_k \left( -\log \left( \frac{\nu_k}{\Delta \tau_k} \right) - \log \left( \frac{\nu_k}{S_k} \right) + 2 \right).$$

As for the Poisson contrast, this based-likelihood contrast is admissible but suffers of the limitation pointed out in the previous section.

Following the same idea, we define a new Marked Poisson-Gamma-Exponential-Gamma (MPGEG) based-likelihood contrast. Precisely, we assume that the  $\lambda_k$ 's and  $\rho_k$ 's are independent random variables and follow a Gamma distribution with parameters  $a_\lambda > 0$  and  $b_\lambda > 0$  and a Gamma distribution with parameters  $a_\rho > 0$  and  $b_\rho > 0$ , respectively. For a fixed  $\boldsymbol{\nu} \in \Upsilon_*^{K, n}$  and for any  $\boldsymbol{\tau} \in \mathcal{P}_\nu^K(N)$ , the MPGEG contrast is

$$\begin{aligned} \gamma_{MPGEG}(\boldsymbol{\tau}) &= -\log p_{MPGEG}(N; \boldsymbol{\tau}, a_\lambda, b_\lambda, a_\rho, b_\rho), \\ &= -\log \iint p_{PGEG}(N, \boldsymbol{\lambda}, \boldsymbol{\rho}; \boldsymbol{\tau}, a_\lambda, b_\lambda, a_\rho, b_\rho) \, d\boldsymbol{\lambda} \, d\boldsymbol{\rho}, \\ &= \sum_{k=1}^K \left( \tilde{a}_{k, \lambda} \log \tilde{b}_{k, \lambda} - \log \Gamma(\tilde{a}_{k, \lambda}) \right) + \left( \tilde{a}_{k, \rho} \log \tilde{b}_{k, \rho} - \log \Gamma(\tilde{a}_{k, \rho}) \right) \\ &\quad + K \left( -a_\lambda \log b_\lambda + \log \Gamma(a_\lambda) - a_\rho \log b_\rho + \log \Gamma(a_\rho) \right), \end{aligned} \tag{14}$$

where  $\tilde{a}_{k, \lambda} = \nu_k + a_\lambda$ ,  $\tilde{b}_{k, \lambda} = \Delta \tau_k + b_\lambda$ ,  $\tilde{a}_{k, \rho} = \nu_k + a_\rho$ , and  $\tilde{b}_{k, \rho} = S_k + b_\rho$ . The derivation of this contrast is detailed in Appendix A. This contrast function is also admissible and can avoid segmentations with zero-length segments.

The posterior means of  $\lambda_k$  and  $\rho_k$  are

$$\hat{\lambda}_k = \tilde{a}_{k, \lambda} / \tilde{b}_{k, \lambda}, \quad \hat{\rho}_k = \tilde{a}_{k, \rho} / \tilde{b}_{k, \rho}.$$

We use these posterior means as estimators of the intensity of the process and of the density parameter of the marks, respectively.

Similarly to the PG contrast, the parameters  $a_\lambda, b_\lambda, a_\rho, b_\rho$  need to be chosen. For the two first parameters, we choose  $a_\lambda = 1$  and  $a_\lambda / b_\lambda = n$ . Then, because the conditional distribution of  $X | N$  a Pareto distribution with parameter  $(b_\rho, a_\rho)$  so  $\mathbb{E}[X | N] = b_\rho / (a_\rho - 1)$  with the condition  $a_\rho > 2$  (to ensure the existence of the variance). Thus, one may choose  $a_\rho = 2.01$  and  $b_\rho = \bar{X}(a_\rho - 1)$ .

## 6 Extension to self-exciting process

In this section, we show that the segmentation of a particular Hawkes-type process can be rewritten as the segmentation of a Poisson process after an adapted transformation.

### 6.1 Model

We consider a self-exciting process  $N$  with conditional intensity process denoted  $\lambda(t)$  at time  $t$ , depending on the entire history before time  $t$ . The compensator or density of this process is represented by  $\Lambda(t)$ . As in the Poisson model, we denote the observed event times within the observation interval  $[0, 1]$  as  $(T_i)_{i \geq 1}$ . We further assume that the intensity in each segment of the partition  $\{I_k = [\tau_{k-1}, \tau_k)\}_{1 \leq k \leq K}$  is the product of a linear exponential Hawkes intensity  $\lambda_0(t)$  and a segment-specific constant. Specifically, the conditional intensity function is defined as follows:

$$\lambda(t) = \sum_{k=1}^K c_k \mathbb{1}_{[\tau_{k-1}, \tau_k)}(t) \lambda_0(t), \text{ with } \lambda_0(t) = \left( 1 + \sum_{T_i < t} \alpha e^{-\beta(t-T_i)} \right), \quad (15)$$

where  $(c_k)_{1 \leq k \leq K}$  is a sequence of positive constants, and the parameters  $\alpha$  and  $\beta$  are positive constants, referred to as the increase rate and the decay rate respectively. For identifiability reasons, the immigration rate of the baseline intensity  $\lambda_0$  is set to 1. It gives the conditional risk of the occurrence of an event at  $t$  given the realization of the process over  $[0, t)$ . For the classical self-exciting Hawkes process ( $c_k = 1$  for all  $k$ ), each arrival in the system instantaneously increases the arrival intensity by  $\alpha$ , then over time this arrival's influence decays at rate  $\beta$ . Here both the immigration rate and the influence of each event on the events to come depend on the segment of arrival. The model (15) can describe the occurrences of self-exciting events, subject to switches of an underlying regime, such as neuronal activity or crime activity, for example. We refer to this model as Piecewise-Hawkes-Process (PHP).

We assume that the process  $N$  satisfies the following assumption.

**Assumption 6.1** (Non-explosion assumption). *The parameters of intensity of the process defined in (15) satisfy*

$$\frac{\alpha}{\beta} \max_k \{c_k\} < 1.$$

The condition comes from the fact that a standard Hawkes process with conditional intensity  $c_{\max} \lambda_0$  doesn't explode if and only if  $\max_k c_k \alpha / \beta < 1$ . Hence, as

$$\lambda(t) \leq \max_k c_k \lambda_0(t),$$

Assumption 6.1 is sufficient to insure that  $\mathbb{E}[N_t] < \infty$  and  $\mathbb{E}[\lambda(t)] < \infty$ . Some details about simulation algorithm through thinning are given in Appendix D. Let us denote for the Hawkes process  $N_0$  with conditional intensity  $\lambda_0(t)$ , the compensator  $\Lambda_0$ , given by the following equation,

$$\Lambda_0(t) := \int_0^t \lambda_0(s) ds = t + \frac{\alpha}{\beta} \sum_{T_i < t} \left( 1 - e^{-\beta(t-T_i)} \right). \quad (16)$$

The link between the process  $N$ , defined by (15), and  $N_0$  is given in Proposition 6.2.

**Proposition 6.2.** *For any  $k \in \{1, \dots, K\}$  and for  $t \in [\tau_k, \tau_{k+1})$ , we have  $\lambda(t) = c_k \lambda_0(t)$  and*

$$\Lambda(t) = c_{k+1} [\Lambda_0(t) - \Lambda_0(\tau_k)] + \sum_{j=1}^k c_j [\Lambda_0(\tau_j) - \Lambda_0(\tau_{j-1})]. \quad (17)$$

We are now able to give method of change-point detection in this model.

## 6.2 Change-point detection strategy

We now describe a strategy to detect the change-points in PHP, which consists in transforming it back into a Poisson process, to which our methodology applies.

**Conversion to a piecewise Poisson process.** The transformation we employ is based on a well-established result for point processes: the random time-change or time-scaling theorem, originally presented in Papangelou (1972) and discussed in works such as Daley and Vere-Jones (2008). Theorem 6.3 provides an adapted version of this theorem specifically for the considered piecewise version of the Hawkes process that we are considering.

**Theorem 6.3** (Modified time-rescaling). *Let  $(T_i)_{i=1}^N$  be the event times observed over  $[0, 1]$  of a PHP with a conditional intensity  $\lambda$  defined by Equation (15), and satisfying Assumption 6.1. Then, the sequence  $(\Lambda_0(T_i))_i$  is a Poisson process with a piecewise constant intensity function  $\lambda_P$  defined as*

$$\lambda_P(t) := \sum_{k=1}^K c_k \mathbb{1}_{[\Lambda_0(\tau_{k-1}), \Lambda_0(\tau_k))}(t). \quad (18)$$

Furthermore, the likelihood of the exponential Hawkes-type process is

$$p_H(N; \boldsymbol{\tau}, \mathbf{c}, \alpha, \beta) = \left( \prod_{i=1}^n \lambda_0(T_i) \right) \left( \prod_{k=1}^K c_k^{n_k} e^{-c_k(\Lambda_0(\tau_k) - \Lambda_0(\tau_{k-1}))} \right). \quad (19)$$

The proof is relegated in Section 11. Let us notice that, because  $\Lambda_0$  is a strictly increasing function (see Laub et al., 2021, Definition 4), the ordering of the event times remains unchanged before and after transformation. Consequently, for each  $k \in \{0, \dots, K-1\}$ , the number of events for the original Hawkes-type process within  $[\tau_k, \tau_{k+1})$  is the same as the number of events for its Poisson version within  $[\Lambda_0(\tau_k), \Lambda_0(\tau_{k+1}))$ . Let us finally mention that the transformed process is not in  $[0, 1]$  anymore but in the random time interval  $[0, \Lambda_0(T_{N[0,1]})]$ . Thus, using Theorem 6.3, we transfer the task of determining the change-points  $(\tau_k)_k$  from  $N$  to a change-point detection problem on the Poisson process  $(\Lambda_0(T_i))_i$  on which the proposed method can be applied. Because the first bracket of the likelihood (19) does not depend on the  $\tau_k$ 's nor on the  $c_k$ 's, the maximization w.r.t the  $\tau_k$  of the obtained Poisson likelihood

$$\prod_{k=1}^K c_k^{n_k} e^{-c_k(\Lambda_0(\tau_k) - \Lambda_0(\tau_{k-1}))}$$

is equivalent to the maximization of the Hawkes-like likelihood (19), for fixed  $\alpha$  and  $\beta$ . Obviously, as seen Section 4, the optimal segmentation according to the Poisson contrast of the transformed process may contain segments with null length, so, in practice, we will use the Poisson-Gamma contrast in place of the Poisson contrast.

**Estimation of  $\alpha$  and  $\beta$ .** The transformation of an exponential PHP into a heterogeneous Poisson process requires to know the parameters  $\alpha$  and  $\beta$ . We describe here two possible strategies. First, we may assume that the process goes through a homogeneous period, that is a period  $[0, T_{\text{learn}}]$  with no change-point. This is the case in some neuronal analyses (see, e.g. Spaziani et al., 2023), where the spiking activity of a mouse is recorded during activity but also during sleep phases, which can therefore be considered as homogeneous. We propose to estimate the parameters  $\alpha$  and  $\beta$  on this homogeneous

period via, for example, maximum likelihood, and to plug them into the compensator (16); denoting  $\hat{\theta} = (\hat{\alpha}, \hat{\beta})$ , we thus define

$$\hat{\Lambda}_0(t) := \Lambda_{0, \hat{\theta}}(t) = 1 + \frac{\hat{\alpha}}{\hat{\beta}} \sum_{T_i < t} \left(1 - e^{-\hat{\beta}(t-T_i)}\right).$$

Algorithm 1 gives the pseudo-code of the PHP change-points detection algorithm (CDPHP) following this strategy.

---

**Algorithm 1** change-points detection for PHP (CDPHP)

---

1: **input**

- $(S_k)_{k=1}^{N_0([0, T_{\text{learn}}])}$  a sample from a HP of conditional intensity  $\lambda_0$  as defined in Equation (15)
- $(T_i)_{i=1}^{N([0, 1])}$  a sample from a PHP of conditional intensity  $\lambda$  as defined in Equation (15)

2: **estimate**  $\theta$  the parameters of  $\lambda_0$  based on  $(S_k)_{k=1}^{N_0([0, T_{\text{learn}}])}$

3: **compute**  $(\hat{\Lambda}_0(T_i))_{i=1, \dots, N([0, 1])}$  (a sequence on  $[0, \hat{\Lambda}_0(T_N)]$ )

4: **find** the set of the  $K$  indexes  $I_K^N$  of the change-points in the sample  $(\hat{\Lambda}_0(T_i))_{i=1}^N$  using a change-point detection method for an inhomogeneous-PP (re-scaled on  $[0, 1]$ )

5: **return**  $\hat{\tau}_1, \dots, \hat{\tau}_K = (T_j)_{j \in I_K^N}$

---

Alternatively, when no homogeneous period is available, we propose to fix  $\beta$  and to run the change-point detection method with a grid of values of  $\alpha$ , keeping the value of  $\alpha$  that maximizes the likelihood function. Several values for  $\beta$  can be then investigated, even if its value is less sensitive. We use this latter strategy in the application presented in Section 9.3.

**Remark 6.4** (Other piecewise point processes.). *The strategy presented in this section, not only applies to exponential Hawkes processes. Indeed, considering a point process with conditional intensity  $\lambda_0(t)$ , any piecewise version of it with conditional intensity  $\lambda(t)$  with the form given in Equation (15) can be segmented with the proposed approach, due to the time-scaling theorem.*

## 7 Choosing the number of segments

Now, let us discuss the selection of the number of segments  $K$ . To address this, we suggest employing a cross-validation strategy that leverages a property of the Poisson process, which we outline for the reader below.

**Property 7.1** (Thinning). *Consider a heterogeneous Poisson process  $N$  with intensity function  $\lambda(t)$ :  $N = \{N_t\}_{0 \leq t \leq 1} \sim PP(\lambda)$ . Sampling each event time of  $N$  with probability  $f$  results in a heterogeneous Poisson process  $N^A$  with intensity function  $\lambda^A(t) = f\lambda(t)$ . Furthermore, the remaining fraction of event times forms a second heterogeneous Poisson process  $N^B$  with intensity function  $\lambda^B(t) = (1-f)\lambda(t)$ , and the processes  $N^A$  and  $N^B$  are independent.*

This thinning property has two important consequences. First, if the intensity function  $\lambda$  is piecewise constant, then the intensity functions  $\lambda^A$  and  $\lambda^B$  are also piecewise constant, *with same change-points as  $\lambda$* . Second, whatever the form of the intensity function of  $N$ , the ratio between the intensity functions of  $N^B$  and  $N^A$  is constant and equal to  $\lambda^B(t)/\lambda^A(t) \equiv (1-f)/f$ . This suggests the following cross-validation procedure: (i) sample events from the observed process  $N$  with probability  $f$

to form a *learning process*  $N^L$  and form an independent *test process*  $N^T$  with the remaining events; (ii) for a series of values of  $K$ , get estimates  $(\hat{\boldsymbol{\tau}}^{K,L}, \hat{\boldsymbol{\lambda}}^{K,L})$  of the change-points and intensities, respectively, using the learning process  $N^L$ , (iii) evaluate the contrast on the test process  $N^T$  with parameters  $(\hat{\boldsymbol{\tau}}^{K,L}, \frac{1-f}{f}\hat{\boldsymbol{\lambda}}^{K,L})$ . Performing thinning  $M$  times gives the following algorithm.

**Algorithm 7.2** (Cross-validation procedure).

**Input:** a realization of the process  $N$ .

**Cross-validation:** for  $m = 1$  to  $M$

1. sample a learning process  $N^{m,L}$  from  $N$  with probability  $f$ , and form the test process  $N^{m,T}$  with the remaining events;
2. for  $K = 1$  to  $K_{\max}$ ,
  - segment the learning process  $N^{m,L}$  using the Poisson-Gamma contrast (11) to get

$$\hat{\boldsymbol{\tau}}^{m,K,L} = \underset{\boldsymbol{\nu} \in \Upsilon_{\star}^{K,n(m,L)}}{\operatorname{argmin}} \min_{\boldsymbol{\tau} \in \mathcal{M}_K^{\nu}(N^{m,L})} \gamma_{PG}(\boldsymbol{\tau}),$$

where  $n(m,L)$  is the number of events in the learning process,

- deduce the estimate  $\hat{\boldsymbol{\lambda}}^{m,K,L}$  as the set of posterior means (12)

$$\hat{\lambda}_k^{m,K,L} = \mathbb{E}(\lambda_k | N^{m,L}, \hat{\boldsymbol{\tau}}^{m,K,L}) = \frac{a^{m,L} + \Delta N_k^{m,L}}{b^{m,L} + \Delta \hat{\tau}_k^{m,K,L}} \quad \text{for all } k = 1, \dots, K,$$

- and compute the Poisson contrast for the test process

$$\gamma^{m,K,T} = -\log p_P \left( N^{m,K,T}; \hat{\boldsymbol{\tau}}^{m,K,L}, \frac{1-f}{f}\hat{\boldsymbol{\lambda}}^{m,K,L} \right).$$

**Averaging:** for  $K = 1$  to  $K_{\max}$ , compute the average contrast

$$\bar{\gamma}^{K,T} = \frac{1}{M} \sum_{m=1}^M \gamma^{m,K,T}.$$

**Selection:** select  $K$  as

$$\hat{K} = \underset{K}{\operatorname{argmin}} \bar{\gamma}^{K,T}.$$

**Some comments.** Few comments can be made about this procedure. First, the algorithm 7.2 involves three tuning parameters: the number of cross-validation sample  $M$ , the maximum number of segments  $K_{\max}$  and the sampling probability  $f$ . The first two are limited only by the computational burden and can be as large as desired. The sampling probability  $f$  was set to 4/5 in this study. Figure 16 in Appendix E shows that this choice yields good performances, as compared to other typical ones.

Second, we use the Poisson-Gamma contrast to estimate the parameters  $\boldsymbol{\tau}$  and  $\boldsymbol{\lambda}$  because it is admissible as explained in Section 4. Still, because the undesirable properties of the Poisson likelihood have no effect when used to measure the fit of  $\hat{\boldsymbol{\tau}}$  and  $\hat{\boldsymbol{\lambda}}$  parameters to an independent process, we use the standard Poisson contrast to evaluate this fit.

Finally, but most importantly, cross-validation is generally not applicable when dealing with discrete-time segmentation problems. Indeed, in this case, it consists in eliminating observation times, which makes the location of the estimated change-point unclear with respect to the complete dataset. The situation is different in the continuous time setting we consider, thanks to the thinning Property 7.1.

**Practical implementation.** In practice, to perform the segmentation of an observed process  $N$ , we propose to first determine  $\widehat{K}$  using the algorithm 7.2, then to estimate  $\boldsymbol{\tau}$  using the Poisson-gamma contrast and  $\boldsymbol{\lambda}$  as the posterior mean on the whole process  $N$ :

$$\begin{aligned}\widehat{\boldsymbol{\tau}} &= \underset{\boldsymbol{\nu} \in \mathcal{T}_*^{\widehat{K}, n}}{\operatorname{argmin}} \min_{\boldsymbol{\tau} \in \mathcal{M}_{\boldsymbol{\nu}}^{\widehat{K}}(N)} \gamma_{PG}(\boldsymbol{\tau}), \\ \widehat{\lambda}_k &= \mathbb{E}(\lambda_k | N, \widehat{\boldsymbol{\tau}}) \quad \text{for all } k = 1, \dots, \widehat{K}.\end{aligned}$$

The adaptation of the algorithm 7.2 to the segmentation of a marked Poisson process is straightforward, replacing the Poisson-Gamma contrast with the marked Poisson-Gamma-Expo-Gamma contrast and the Poisson contrast with the marked Poisson contrast, respectively.

## 8 Simulation study

We present in this section a simulation study to evaluate the performances of the proposed methodology. In Section 8.1 we explain the investigated cases, and in Section 8.2 we give the result when the simulation is done under the Poisson model, the marked-Poisson model or the Hawkes model (PHP).

### 8.1 Simulation design and quality criteria

**Poisson process.** We use a simulation design for the change-points inspired from Chakar et al. (2017). We set the number of segments to  $K = 6$ , with  $\boldsymbol{\tau} = [0, 7, 8, 14, 16, 20, 24]/24$  change-point locations, i.e. with lengths  $\Delta\boldsymbol{\tau} = [7, 1, 6, 2, 4, 4]/24$ . The total length of odd segments ( $k = 1, 3, 5$ ) is  $\Delta\tau_- = 17/24$  and the total length of even segments is  $\Delta\tau_+ = 7/24$ . The intensity is set to  $\lambda_-$  in odd segments and to  $\lambda_+$  in even segments, based on the two following parameters:

$\bar{\lambda}$  : mean intensity:  $\bar{\lambda} = \int_0^1 \lambda(t) dt = (\lambda_- \Delta\tau_- + \lambda_+ \Delta\tau_+)$ . It controls the expected number of events. A small value for  $\bar{\lambda}$  yields a very scarce signal, i.e. a very poor available information. We consider the values  $\bar{\lambda} = 32, 56, 100, 178, 316, 562$  and 1000.

$\lambda_R$  : ratio between even and odd intensities:  $\lambda_R := \lambda_+ / \lambda_- \geq 1$ . It controls the contrasts between successive segments. Note that  $\lambda_R = 1$  actually yields a single segment with intensity  $\bar{\lambda}$ . We consider the values  $\lambda_R = 1, 2, 3, 4, 6, 8, 11$  and 16.

The values of the intensities  $\lambda_-$  and  $\lambda_+$  are then  $\lambda_- = \bar{\lambda} / (\Delta\tau_- + \lambda_R \Delta\tau_+)$  and  $\lambda_+ = \lambda_R \lambda_-$ . Examples of such piecewise intensity functions  $\lambda$  are given in Figure 2 for  $\bar{\lambda} = 100$  and three values of  $\lambda_R$ . The values of  $\lambda_-$  and  $\lambda_+$  deduced for all the considered values of the mean intensity  $\bar{\lambda}$  and the ratio  $\lambda_R$  are given in Table 2 in Appendix C, together with a measure, called SNR, we defined to evaluate the difficulty of the detection problem.

The maximum number of segments is  $K_{\max} = 12$ . We use  $M = 500$  samples for the cross-validation procedure and the sampling probability is set to  $f = 4/5$ .  $B = 100$   $N$  processes are sampled with each parameter configuration. For the Poisson-Gamma contrast, we take the hyper-parameters  $a = 1$  and  $b = 1/n$ , where  $n$  is the number of events in the process to be segmented.

**Marked Poisson process.** The aim here is to see if the additional change-point information carried by the mark process helps the detection, and to know which of the two processes (the Poisson process and the mark process) allows better detection of the change-points. We use the same simulation design as previously for the change-point locations, fixing  $\bar{\lambda} = 100$ . We consider two values for  $\lambda_R$ :  $\lambda_R = 1$  where the ground intensity of the Poisson process does not change from a segment to another, no signal in  $\lambda$ , and  $\lambda_R = 8$  where the change in the intensity is marked, signal in  $\lambda$ . For each value of

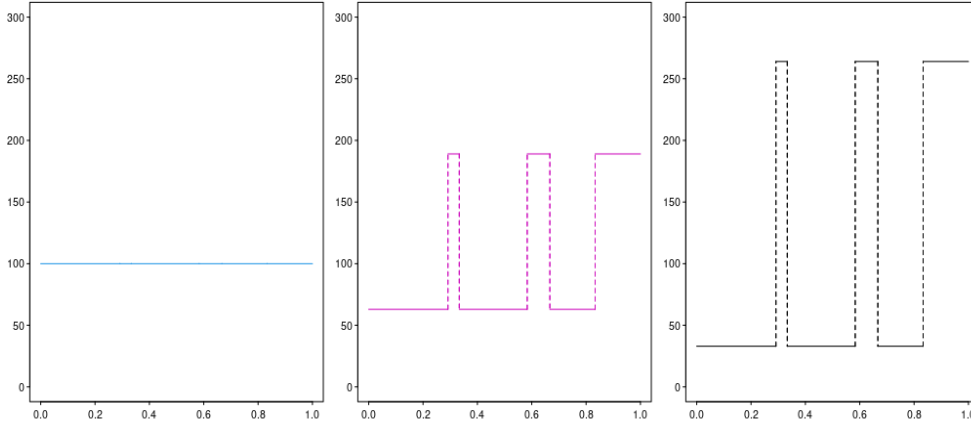


Figure 2: Piecewise intensity function  $\lambda(t)$  on  $[0, 1]$  for  $\bar{\lambda} = 100$  and  $\lambda_R \in \{1, 3, 8\}$  from left to right.

$\lambda_R$ , the parameter of the mark distribution  $\rho(t)$  is either constant and equals to 0.1, no signal in  $\rho$ , or alternates between 0.1 and 0.005 for the odd and the even segments respectively, signal in  $\rho$ . This leads to four scenarios in terms of detection according to the existence, or not, of changes in either  $\lambda$  or  $\rho$ .

**Piecewise Hawkes-type process.** We study the performance of the change-point detection in a piecewise Hawkes-type process, described in Section 6. We use the same segmentation  $\tau$  as in the Poisson case and transfer the difficulty of the change-point detection task on the values of  $c_k$  involved in the intensity (15). The parameters  $c_k$  are set to  $c_-$  in odd segments and to  $c_+$  in even segments; we considered three values for the ration  $R = c_+/c_-$ :  $R \in \{2, 3, 6\}$ . We fixed  $\alpha = 0.5$ ,  $\beta = 500$  and  $c_+ = 500$  (thus, for  $R = 2, 3, 6$ , we have  $c_- = 333, 250, 142.8$ , respectively). By analogy with the stationary regime on each interval (under which the expected number of points is  $c_k/(1 - c_k\alpha/\beta)$ ), these parameters correspond to the pink curve displayed for the Poisson process on Figure 4 ( $\bar{\lambda} = 562$ ).

We investigate the case where the parameters  $(\alpha, \beta)$  are known (named "known" in Figure 7) and the case where they are estimated using maximum likelihood on a homogeneous period with length  $T_{\text{learn}} \in \{1, 10\}$  and intensity  $c_0\lambda_0(t)$ , where  $c_0 = 100$ .

**Quality criteria.** The performances are assessed according to the following criteria.

- The selected number of segments  $\hat{K}$  (obtained with Algorithm 7.2).
- The Hausdorff distance  $d(\tau, \hat{\tau})$  between the true change-point locations  $\tau$  and the estimated ones  $\hat{\tau}$  (with possibly different number of change-points, as in Chakar et al. (2017)). More specifically, defining

$$d_1(\tau, \hat{\tau}) = \max_k \min_\ell |\tau_k - \hat{\tau}_\ell|, \quad d_2(\tau, \hat{\tau}) = d_1(\hat{\tau}, \tau),$$

$$d(\tau, \hat{\tau}) = \max(d_1(\tau, \hat{\tau}), d_2(\tau, \hat{\tau})),$$

$d_1$  indicates if each true change-point  $\tau_k$  is close to an estimated one  $\hat{\tau}_\ell$  ( $d_1$  will typically be small when  $\hat{K} \gg K$ ), whereas  $d_2$  indicates if each estimated change-point  $\hat{\tau}_\ell$  is close to a true one  $\tau_k$ . A perfect segmentation results in both null  $d_1$  and  $d_2$  (and  $d = 0$ ).

- The relative  $L^2$ -norm between the estimated and the true cumulative intensity functions. More specifically, denoting  $\lambda(t)$  and  $\hat{\lambda}(t)$  the true and estimated intensity functions respectively and

$\Lambda(t) = \int_0^t \lambda(u)du$  and  $\widehat{\Lambda}(t) = \int_0^t \widehat{\lambda}(u)du$  the corresponding cumulative intensity functions, we compute:

$$\ell^2(\Lambda, \widehat{\Lambda}) = \left( \int_0^1 (\widehat{\Lambda}(t) - \Lambda(t))^2 dt \right) / \bar{\lambda}.$$

## 8.2 Results

We present first the results for the piecewise homogeneous Poisson process model.

**Model selection.** Figure 3 shows the mean number of the selected number of segments  $\widehat{K}$  as a function of  $\lambda_R$  (a measure of the difficulty of the task). The correct number of segments  $K = 6$  is better recovered when either the mean intensity  $\bar{\lambda}$  or the ratio  $\lambda_R$  increases, as expected. More precisely, for a high mean intensity ( $\bar{\lambda} = 1000$ ), the correct number of segments  $K = 6$  is recovered as soon as the ratio  $\lambda_R$  reaches 3. In the typical case where  $\bar{\lambda} = 100$ , the correct number of segments is obtained when  $\lambda_R$  is about 10. When  $\lambda_R = 1$ , for all  $\bar{\lambda}$ , the mean number of the selected number of segments  $\widehat{K}$  is found to be 1, which is actually the correct number (as the intensity is constant in this case). When  $\lambda_R$  is slightly greater than one, especially for small mean intensities  $\bar{\lambda}$ , the model selection procedure tends to underestimate the number of segments. This behavior is classical and desired to avoid false detection (see e.g. Cleynen and Lebarbier, 2017).

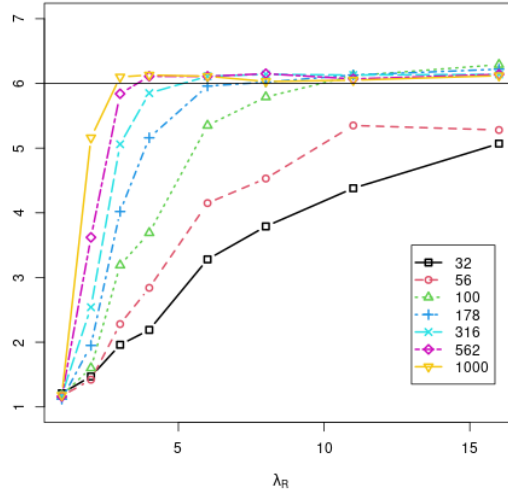


Figure 3: Mean selected number of segments  $\widehat{K}$  (averaged over  $B = 100$  replicates) as a function of the intensity ratio  $\lambda_R$ . Legend panel = value of the mean intensity  $\bar{\lambda}$ .

**Accuracy of the change-points.** The left panel of Figure 4 represents the average of the Hausdorff distance as a function of the ratio  $\lambda_R$ . It shows the expected behavior in terms of accuracy of the locations of the estimated change-points. The Hausdorff distance  $d(\boldsymbol{\tau}, \widehat{\boldsymbol{\tau}})$  decreases as either the mean intensity  $\bar{\lambda}$  or the ratio  $\lambda_R$  increases. The distance is almost zero with a mean intensity  $\bar{\lambda} = 1000$  and a ratio  $\lambda_R = 3$ . In the typical case where  $\bar{\lambda} = 100$ , the distance decreases very quickly as  $\lambda_R$  increases, but remains above .05, meaning that some uncertainty remains about the precise locations of the change point. Note that when  $\lambda_R = 1$ , the Hausdorff distance is almost 0 for all values of  $\bar{\lambda}$ ,



simply because the selected number of segments is almost always 1, giving  $\hat{\tau} = \{0, 1\}$ , which is equal to the true  $\tau$ .

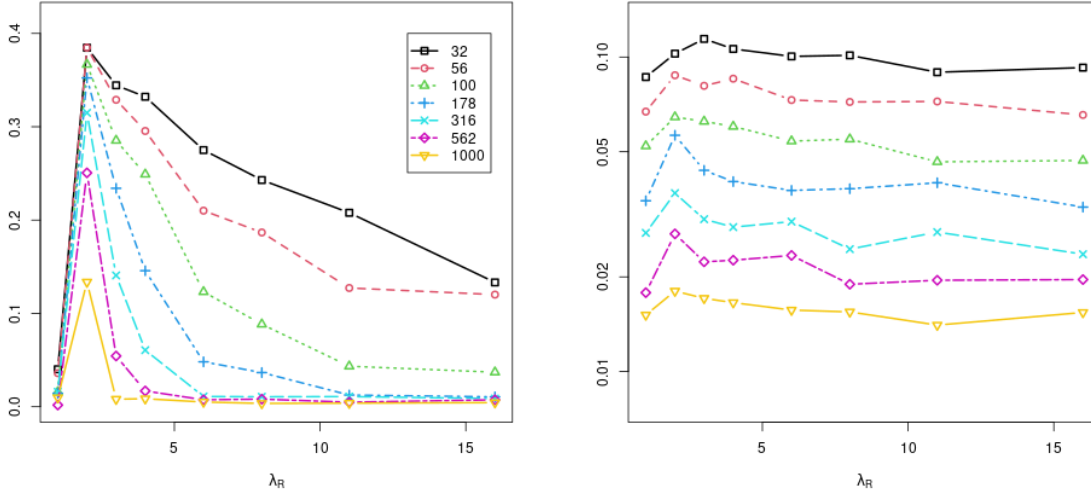


Figure 4: Left: Mean Hausdorff distance  $d(\tau, \hat{\tau})$  as a function of the ratio  $\lambda_R$ . Legend panel = value of the mean intensity  $\bar{\lambda}$ . Right: Mean relative distance  $\ell_2(\Lambda, \hat{\Lambda})$  between the true and estimated cumulated intensity function  $\Lambda(t)$  as a function of the ratio  $\lambda_R$  (same legend as left panel).

The Hausdorff distance gives a synthetic measure of the proximity between the estimated change-points  $\hat{\tau}$  and the true ones  $\tau$ . To better illustrate the accuracy of the position of the estimated change-points, for a given configuration  $(\bar{\lambda}, \lambda_R)$ , we gather all the detected change-points resulting from the  $B = 100$  simulations. Figure 5 displays the distribution of the estimated locations for three configurations, chosen according to the results displayed in Figure 4 (left):  $\bar{\lambda} = 56, \lambda_R = 6$  (hard setting),  $\bar{\lambda} = 100, \lambda_R = 8$  (intermediate setting),  $\bar{\lambda} = 316, \lambda_R = 11$  (easy setting). The figure shows how the estimated  $\hat{\tau}_k$  concentrates around the true  $\tau_k$  as the signal becomes more contrasted. Note that the simulation procedure includes the selection of the number of segments  $K$ , so the different simulations do not provide the same number of estimated change-points  $\hat{\tau}_k$ , which explains why the total number of estimated change-points varies from one configuration to another.

**Estimation of the intensity function.** The right panel of Figure 4 represents the mean relative  $\ell_2$  distance between the true and the estimated cumulated intensity function, as a function of the ratio  $\lambda_R$ . It shows that the estimation of the cumulated intensity function  $\Lambda$  improves as the mean intensity  $\bar{\lambda}$  increases. More interestingly, the ratio  $\lambda_R$  does not seem to strongly affect the accuracy of  $\hat{\Lambda}$ . A possible explanation is that although a strong contrast between the intensity of neighboring segments gives better localization of the change-points, even a small error in the change-point location induces a high error in terms of  $\lambda(t)$  or  $\Lambda(t)$ .

**Results for the marked Poisson process.** Table 1 gives the average of the selected number of segments  $\hat{K}$  and the average of the Hausdorff distance  $d(\tau, \hat{\tau})$  for the four scenarios described in Section 8.1. When both the intensity and the mark parameters are constant, the average of  $\hat{K}$  is close to 1, which is the true number, and thus the average of the Hausdorff distance is close to 0. This shows that the procedure is not prone to overfit by detecting non-existing change-points.

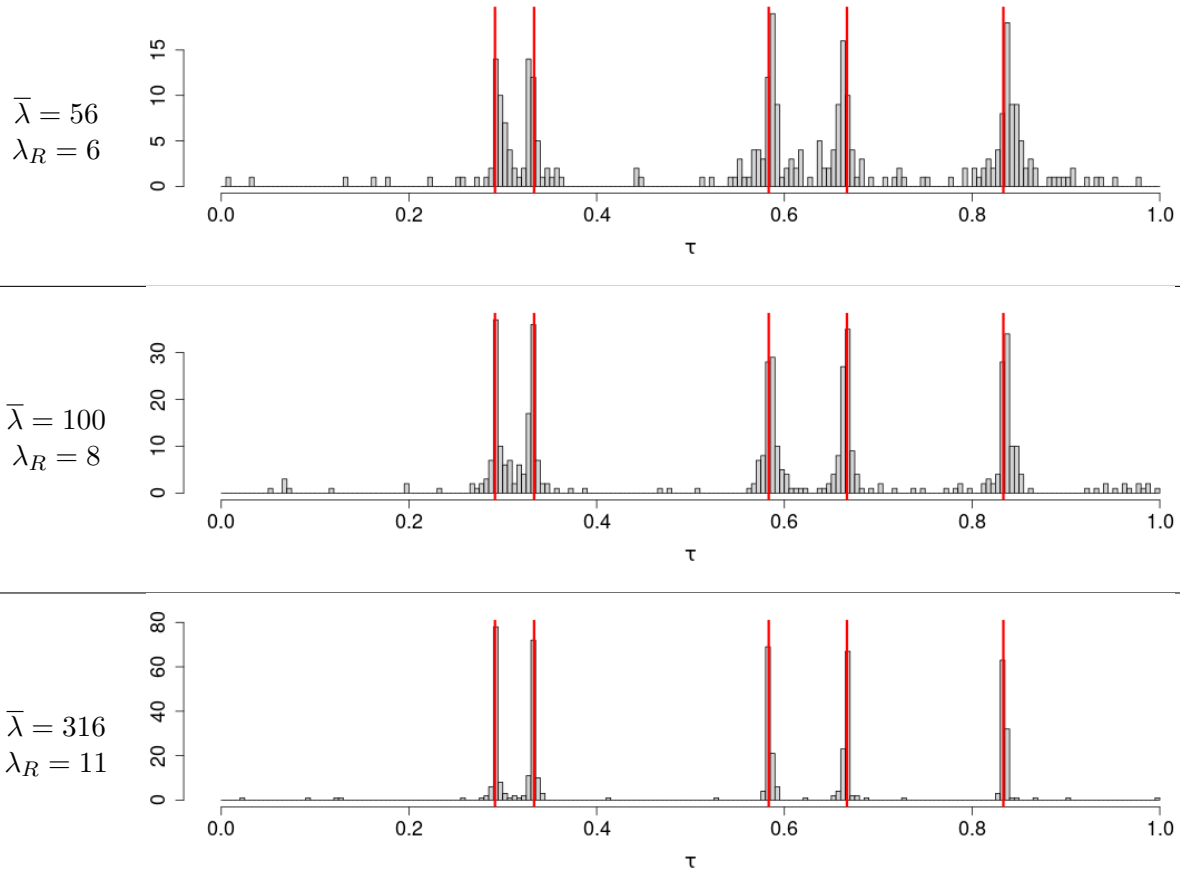


Figure 5: Distribution of the estimated change-point locations  $\hat{\tau}_k$  across the  $B = 100$  simulations for three different settings. Top:  $\bar{\lambda} = 56, \lambda_R = 6$ , center:  $\bar{\lambda} = 100, \lambda_R = 8$ ; bottom:  $\bar{\lambda} = 316, \lambda_R = 11$ . Vertical red lines: true change-point locations  $\tau$ .

Table 1: Mean selected number of segments  $\hat{K}$  and mean Hausdorff distance  $d(\tau, \hat{\tau})$ , from 200 repetitions.

$\lambda \setminus \rho$	$\hat{K}$		$d(\tau, \hat{\tau})$	
	no signal	signal	no signal	signal
no signal	1.132	5.796	0.411	0.126
signal	5.411	5.998	0.112	0.056

When both processes are significantly affected by the changes, the correct number of segments ( $K = 6$ ) is recovered and the estimated change-points is close to the true one (and the Hausdorff distance is close to 0). Interestingly, in terms power to detect change-points, there is no clear distinction between the cases where the signal is only in  $\lambda$  or only in  $\rho$ , but the existence of a signal in both parts of the process increases this power.

**Results for the piecewise Hawkes-type process.** Figure 6 shows the estimated change-point in plain red lines and the true one in dotted red lines for a specific PHP with ratio  $R = 3$ . The summary

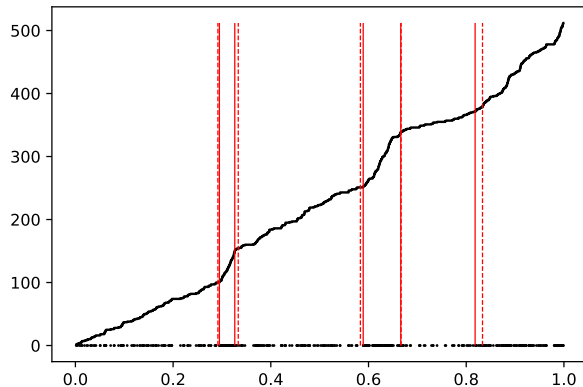


Figure 6: Example with  $R = 3$ . The counting process is the black line, with the events on the x-axis, the true change-points are the plain red lines and the estimated change-points are the dotted red lines.

of the results for the Hausdorff distance are presented in Figure 7. The boxplots labeled "known" refer to the cases where the parameters  $(\alpha, \beta)$  are known and given to the algorithm. We represent here three boxplot for each value of  $R \in \{2, 3, 6\}$ . As expected, the lower is  $R$ , the harder is the task and, thus, the higher is the Hausdorff distance. We observe that the results when the coefficients are known are similar to those obtain for the pink curve on Figure 4 for the Poisson process (which corresponds to the closest scenario in terms of parameters). Then, when the parameters have to be estimated on a period  $[0, T_{\text{learn}}]$ , the mean Hausdorff distance for the estimated sequence of change-points is close to the one obtained when the parameters  $(\alpha, \beta)$  are known, and even remarkably close for  $T_{\text{learn}} = 10$ . This suggests that the proposed transformation of the process is actually efficient to detect change-points in a piecewise Hawkes-type processes.

## 9 Illustrations in vulcanology and seismology

In this section, for illustration, we analyze two datasets describing volcano activity. In Section 9.1, only the eruption dates are taken into account and we look for homogeneous segments in a Poisson process. In Section 9.2, the duration of each eruption is also considered and we look for change-points in a marked Poisson process.

### 9.1 Poisson process

We consider the eruptions of the Kilauea and Mauna Loa volcanoes in Hawaii, presented by Ho and Bhaduri (2017). Both datasets include recorded eruption dates from 1750 to 1983 for Kilauea Volcano and through 1984 for Mauna Loa Volcano. Over these periods,  $n = 63$  eruptions were observed for

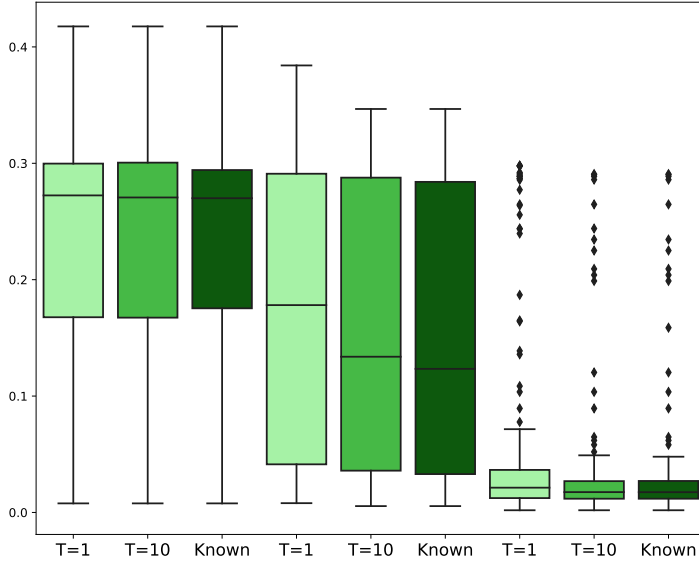


Figure 7: Boxplot of the Hausdorff distance for 200 repetitions for  $R \in \{2, 3, 6\}$ .

the first and  $n = 40$  for the second. The original data only reports the number of eruptions per year (ranging from 0 to 4). Continuous times were reestablished by associating each eruption with a uniformly distributed date, in the corresponding year.

Figure 8 provides the values of the cross-validation criterion  $\bar{\gamma}^{K,T}$  as a function of  $K$  defined in Section 7 for each series of eruption dates. The criterion indicates the existence of four segments for the Kilauea and two segments (i.e. one change-point) for the Mauna Loa volcano. Note that this last criterion admits a local minimum at  $K = 4$ .

Figure 9 gives the optimal segmentation of the Kilauea series in  $K = 4$  segments (three change-points located at the years 1918, 1934, 1952) and of the Mauna Loa series  $K = 2$  segments (one change-point located at the year 1843). We observe a better fit for the Kilauea series than for the Mauna Loa series. This may result from a conservative behavior of the model selection procedure when the number of events is small ( $n = 63$  for the Kilauea volcano and  $n = 40$  for the Mauna Loa volcano). Figure 17 in Appendix F shows the segmentations of the Mauna Loa series with  $K = 3, 4, 5$  and 6 segments.

## 9.2 Marked Poisson process

The data comes from the technical report (Passarelli et al., 2010). It consists in mount Etna volcano flank eruption data between 1607 and 2008. Indeed, flank eruption constitutes one of the most important threat for an assessment of volcanic risk according to the authors. The first variable is the date of the eruption of the volcano located in the North Eastern part of the Sicily Island, and the second one is the volume of lava spread. There are  $n = 63$  events.

We study these data with the inhomogeneous Poisson model then with the marked Poisson model that we presented previously. We search for the best number of segments  $K$  in the collection  $\{1, \dots, 10\}$ . The chosen dimension is  $\hat{K} = 2$  with both models. The two contrast functions are shown in Figure 10 and the obtained segmentations are given in Figure 11. We see that the segmen-

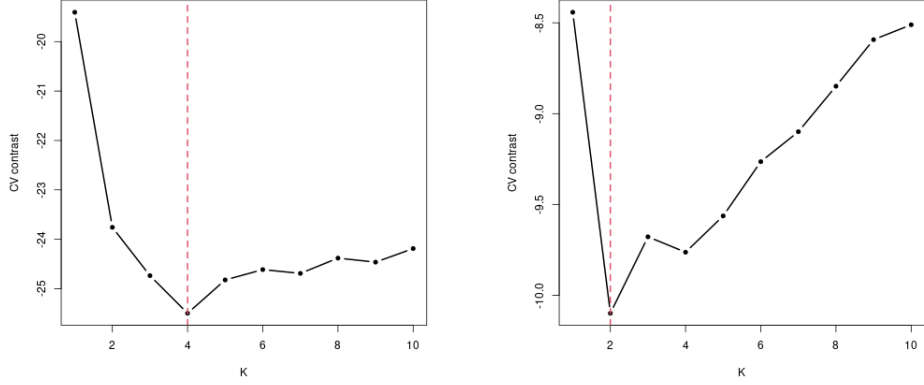


Figure 8: Eruptions of the Kilauea (left) et Mauna Loa (right) volcanos. Selection of the number of segments  $K$ : black solid-bullet line = criterion  $\bar{\gamma}^{K,T}$ , vertical red dotted line = optimal number of segments  $\hat{K}$ .

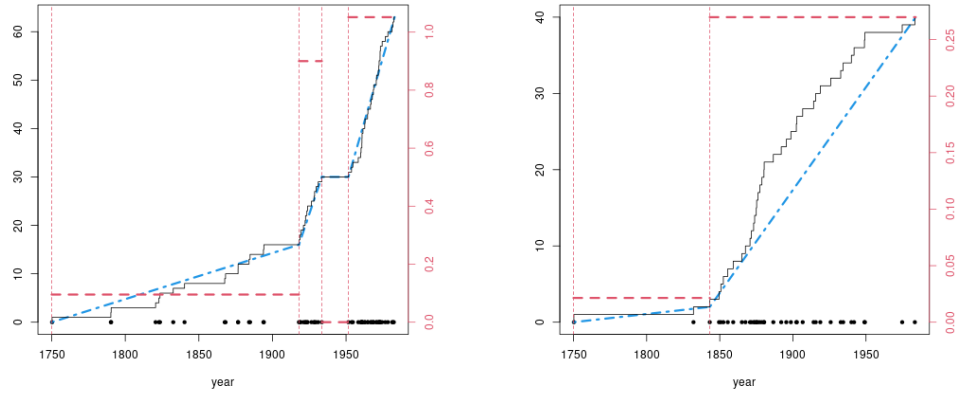


Figure 9: Eruptions of the Kilauea (left) et Mauna Loa (right) volcanos. Final segmentation: black bullets = eruptions times  $T_i$ , black solid line = observed count process  $N(t)$ , red vertical dotted lines = estimated change points  $\hat{\tau}_k$ , blue dotted-dashed line = estimated cumulated intensity  $\hat{\Lambda}(t)$ , red dashed horizontal lines = estimated piecewise constant intensity  $\hat{\lambda}(t)$  (referred to the right axis). The first vertical red dotted lines is  $\tau_0 = 0$ .

tations are different and we believe that we can see the influence of the mark on the second graph. Indeed, on the one hand the Poisson model without marks chooses a change-point at 1968 because after that (as it is explained for example in Tanguy et al. (2007)) the eruptions occur very closely in time until 2001, which justifies a change of regime. On the other hand, the marked process chooses a change-point at 1755, probably mainly because the marks are larger before this time than after (indeed, the report (Tanguy et al., 2007) explains that probably the lava measured after 1755 was mostly buried under the products of additional activity). Furthermore, in Figure 12 where we represent the segmentation obtained with the marked Poisson model, imposing  $K = 3$ , we can see that the method gives a segmentation with two change-points which are close to the single change-point found by the Poisson process model and the single change-point found by the marked Poisson process model.

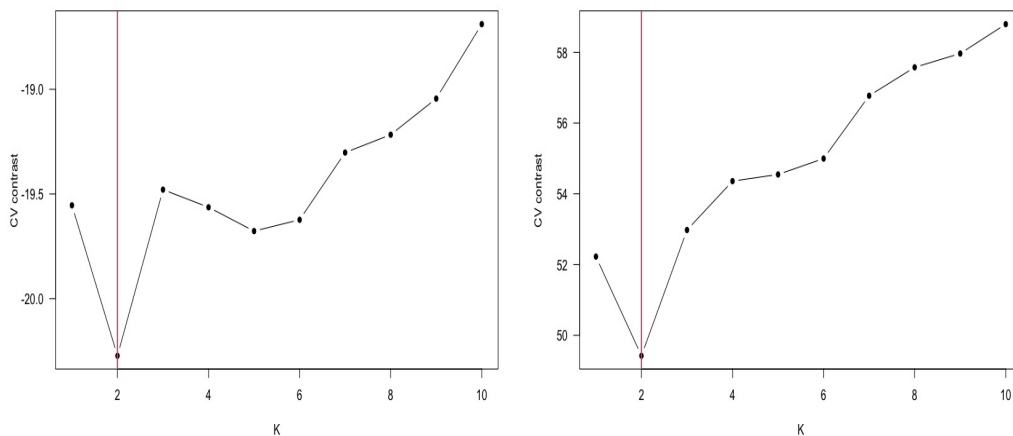


Figure 10: Eruptions of Etna. Left graph: Poisson model, right graph: marked Poisson model. Contrast function as a function of  $K$ , and in red the selected dimension  $\hat{K} = 2$  in both cases.

### 9.3 Self-exciting process

We now examine the sequence of earthquakes and aftershocks in Thailand, described in Harte (2010), and available in the R-package `PtProcess`. The complete dataset includes the magnitudes of the shocks, which we use here solely to characterize the main events to be detected. The three significant events are the earthquakes that occurred in Phuket in December, 25, 2004, and in Sumatra in March, 28, 2005, and September, 12, 2007, corresponding to the largest magnitudes (around 8.5) as shown in the right panel of Figure 13. We apply the PHP model to detect these main events using only the recorded occurrences, excluding the magnitudes. Since the parameters of the underlying process,  $\theta$ , are unknown, we first fix the parameter  $\beta$  and then run the algorithm over a grid of  $\alpha$  values, selecting the one that maximizes the log-likelihood.

Initially, we analyzed the observed process within a Poisson framework (as outlined in Sections 2, 3 and 4), but were unable to identify the three main events, even with a larger number of change-points. We then shifted to the PHP model, estimating the parameters  $\alpha$  and  $\beta$  using the second method described at the end of Section 6, with  $K = 5$  segments. We observed a minimal influence of the  $\beta$  value on the change-point detection on this example in this example, so we fixed it at 8. The results shown in Figure 13 indicate that we accurately detected the three main events (with 15 days of delay for the second one. We detect an additional event on September, 29, 2007, which seems to ends a very high seismic activity.

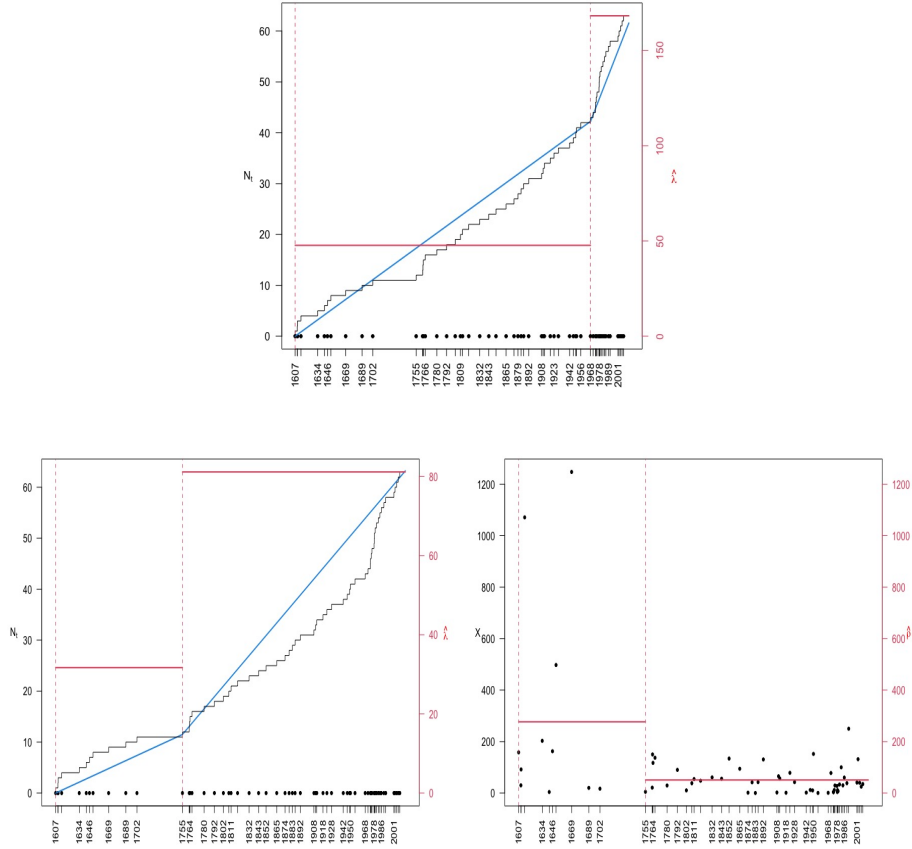


Figure 11: Eruptions of Etna. Top line: Poisson model, bottom line: marked Poisson model. (Left graphs) Final segmentations: black bullets = eruptions times  $T_i$ , black solid line = observed count process  $(N_t)$ , red vertical dotted lines = estimated change points  $\hat{\tau}_k$ , blue dotted-dashed line = estimated cumulated intensity  $\hat{\Lambda}(t)$ , red dashed horizontal lines = estimated piecewise constant intensity  $\hat{\lambda}(t)$  (referred to the right axis). Bottom right graph: black bullets = marks  $X_i$ , red vertical dotted lines = estimated change points, red dashed horizontal lines = estimated piecewise constant parameter of the exponential distribution of the marks  $\hat{\rho}$ .

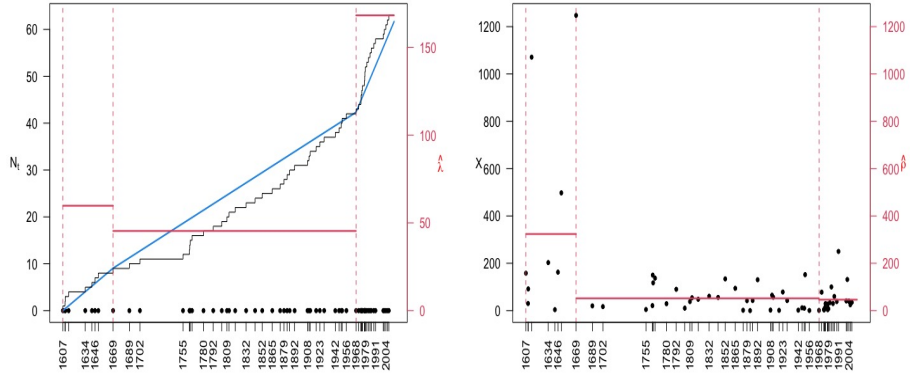


Figure 12: Eruptions of Etna. Marked Poisson model. Same legend as top line of Figure 11 with  $K = 3$ .

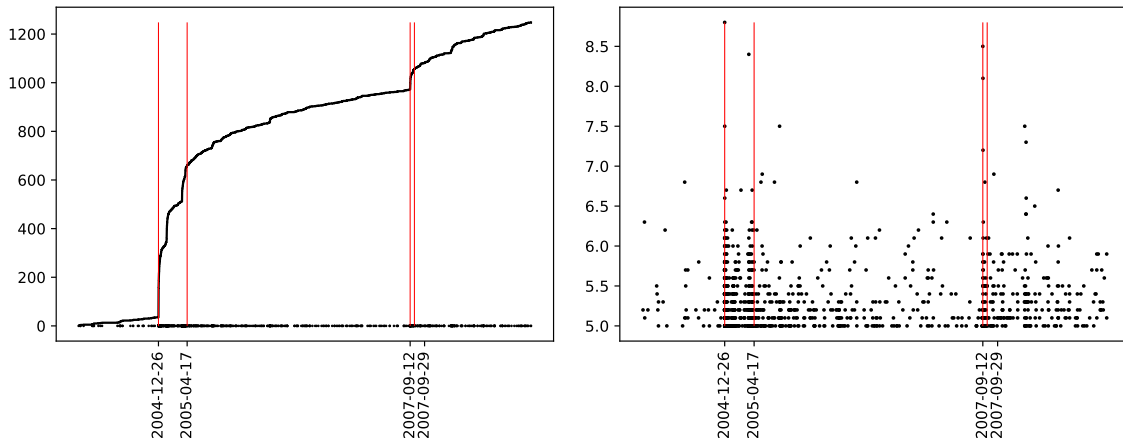


Figure 13: Aftershock sequence of the Phuket earthquake. Counting process (black line) and events (dots), together with estimated change-points in red lines and the dates on the  $x$ -axis. Right graph: magnitudes (not used of the estimation).



## 10 Discussion

We present a comprehensive frequentist framework for detecting multiple change-points in the intensity of a Poisson process. As is common in change-point detection, the inference procedure consists of two steps: (1) segmenting the observed path  $N$  into a predetermined number of segments, and (2) selecting this number. For step (1), we demonstrate that any contrast function satisfying both segment-additivity and concavity allows for the optimal segmentation into  $K$  segments to be achieved exactly and efficiently using a dynamic programming algorithm. Note that the use of dynamic programming fundamentally relies on the segment-additivity property and that traditional methods like maximum likelihood or least-square inference fit within this framework. For step (2), we propose employing a cross-validation strategy

Most model selection criteria for determining the number of segments  $K$  involve penalized contrasts, where the penalty term is dependent on  $K$  (as in the classical BIC and AIC, or in Lebarbier, 2005; Lavielle, 2005; Jackson et al., 2005; Killick et al., 2012) or both on the number of segments and their lengths Zhang and Siegmund (2007). As noted by Jackson et al. (2005), if the penalty term is proportional to  $K$ , it can be spread in the cost of each segment, allowing for the integration of both tasks into a single dynamic programming step, thus achieving segmentation and model selection simultaneously. Our framework can also include more general penalized contrasts, provided that the penalty also satisfies the same admissibility condition.

The computational cost of dynamic programming is quadratic in the number of events  $n$  and linear in the number of segments  $K$ , that is  $\mathcal{O}(n^2K)$ , which can be too demanding when dealing with a large number of events. Time efficiency can be enhanced by utilizing the pruned version of dynamic programming proposed by Killick et al. (2012), which yields a complexity almost linear in  $n$ .

Finally, in many scenarios, multiple simultaneous trajectories are observed. In such cases, detecting changes that affect all series concurrently becomes the goal. If the associated contrast remains concave with respect to segment lengths, this problem can be addressed with a complexity comparable to that of the univariate case.

## 11 Proofs

### 11.1 Proofs of Proposition 3.3

Let fix  $\nu \in \Upsilon_{\star}^{K,n}$  and take  $\tau \in \mathcal{M}_{\nu}^K(N)$ . Denoting by  $C'$  and  $C''$  the first and second derivative of  $C$  with respect to its second argument, we have, for all  $1 \leq k < K$ ,

$$\begin{aligned} \frac{\partial \gamma(\tau)}{\partial \tau_k} &= C'(\nu_k, \Delta\tau_k) - C'(\nu_{k+1}, \Delta\tau_{k+1}), & \frac{\partial^2 \gamma(\tau)}{\partial \tau_k \partial \tau_{k+1}} &= -C''(\nu_{k+1}, \Delta\tau_{k+1}) \quad (\text{if } k < K - 1), \\ \frac{\partial^2 \gamma(\tau)}{\partial \tau_k^2} &= C'''(\nu_k, \Delta\tau_k) + C'''(\nu_{k+1}, \Delta\tau_{k+1}). \end{aligned}$$

The Hessian matrix of the contrast  $\gamma$  is the following  $(K - 1) \times (K - 1)$  matrix

$$H_K = \begin{pmatrix} -(A_1 + A_2) & A_2 & 0 & \dots & \\ A_2 & -(A_2 + A_3) & A_3 & \dots & \\ 0 & \ddots & \ddots & \ddots & \\ \vdots & 0 & A_{K-1} & -(A_{K-1} + A_K) & \end{pmatrix},$$

where  $A_k := -C''(\nu_k, \Delta\tau_k)$ . For all vector  $u \in \mathbb{R}^{K-1} \setminus \{0\}$ , we have that

$$\begin{aligned} u^t H_K u &= - \sum_{k=1}^{K-1} u_k^2 (A_k + A_{k+1}) + 2 \sum_{k=1}^{K-2} u_k A_{k+1} u_{k+1}, \\ &= - \sum_{k=1}^{K-2} (u_k - u_{k+1})^2 A_{k+1} - u_1^2 A_1 - u_{K-1}^2 A_K. \end{aligned}$$

Using the concavity Assumption 3.2 of the contrast function on each segment we have that  $A_k \geq 0$  for all  $k$ , thus  $u^t H_K u \leq 0$ , which concludes the proof.

## 11.2 Proof of Proposition 6.2

If  $t \in [\tau_k, \tau_{k+1}[$ ,

$$\Lambda(t) = \int_0^t \lambda(u) du = \int_0^t \sum_{\ell=1}^{k+1} c_\ell \mathbb{1}_{[\tau_{\ell-1}, \tau_\ell[}(u) \lambda_0(u) du$$

then

$$\begin{aligned} \Lambda(t) &= \sum_{\ell=1}^k c_\ell \int_{\tau_{\ell-1}}^{\tau_\ell} \lambda_0(u) du + c_{k+1} \int_{\tau_k}^t \lambda_0(u) du \\ &= \sum_{\ell=1}^k c_\ell (\Lambda_0(\tau_\ell) - \Lambda_0(\tau_{\ell-1})) + c_{k+1} (\Lambda_0(t) - \Lambda_0(\tau_k)). \end{aligned}$$

## 11.3 Proof of Theorem 6.3

Denoting by  $T_1, \dots, T_n$  the event times of the Hawke-type process  $N$  defined in Section 6, and by  $(H_t)_t$  the history of the process, the likelihood of  $N$  is

$$f_N(T_1, \dots, T_n) := p_H(N; \boldsymbol{\tau}, \mathbf{c}, \alpha, \beta) = \left( \prod_{i=1}^n \lambda(T_i) \right) e^{-\int_0^1 \lambda(s) ds}.$$

We now split the interval  $[0, \tau_K)$  into the intervals  $I_k = [\tau_{k-1}, \tau_k)$  for  $k = 1, \dots, K$ . Denoting by  $n_k$  the number of event times that occur in interval  $I_k$ , because  $\lambda(t) = c_k \lambda_0(t)$  within segment  $I_k$ , we get

$$\begin{aligned} f_N(T_1, \dots, T_n) &= \prod_{k=1}^K \left( \prod_{T_i \in I_k} \lambda(T_i) \right) e^{-\int_{\tau_{k-1}}^{\tau_k} \lambda(s) ds} \\ &= \left( \prod_{i=1}^n \lambda_0(T_i) \right) \left( \prod_{k=1}^K c_k^{n_k} e^{-c_k (\Lambda_0(\tau_k) - \Lambda_0(\tau_{k-1}))} \right), \end{aligned} \quad (20)$$

which gives Equation (19).

For event times  $(t_i)_i$ , we define the transformed inter-event times  $u_i := \Lambda_0(t_i) - \Lambda_0(t_{i-1})$ , for  $i \in \{1, \dots, n\}$  (with  $t_0 = 0$ ),  $\psi$  as the function defined over the cube  $[0, \tau_K)^n$  by

$$\psi : (t_1, \dots, t_n) \mapsto (u_1, \dots, u_n)$$

and  $J_\psi$  as its Jacobian matrix. Using a multivariate change of variable theorem, the joint density function  $f_{\mathbf{u}}$  of  $\{u_1, \dots, u_n\}$  is

$$f_{\mathbf{u}}(u_1, \dots, u_n) = f_N(\psi^{-1}(u_1, \dots, u_n)) / |J_\psi(\psi^{-1}(u_1, \dots, u_n))|, \quad (21)$$

This change of variable is valid because the function  $\psi$  is one-to-one, and the Jacobian determinant  $|J_\psi(t_1, \dots, t_{n_k})|$  does not vanish, allowing us to obtain (21). The first assertion is straightforward as  $\Lambda_0$  is a bijective function. The second assertion can be confirmed by observing that  $J_\psi(t_1, \dots, t_n)$  is a lower triangular matrix, leading to its determinant being the product of its diagonal elements, that is

$$|J_\psi(t_1, \dots, t_n)| = \prod_{k=1}^K \prod_{t_i \in I_k} \frac{\lambda(t_i)}{c_k} = \prod_{i=1}^n \lambda_0(t_i), \quad (22)$$

which doesn't vanishes since  $\lambda(t) > 0$  and  $c_k > 0$  by assumption. Inserting (20) and (22) in expression (21), we get

$$f_{\mathbf{u}}(u_1, \dots, u_n) = \prod_{k=1}^K c_k^{n_k} e^{-c_k(\Lambda_0(\tau_k) - \Lambda_0(\tau_{k-1}))}$$

which is the joint distribution of the inter-event times of an heterogeneous Poisson process with piecewise constant intensity (15).

## Acknowledgments

This work has been conducted within the FP2M federation (CNRS FR 2036). This work is also part of the 2022 DAE 103 EMERGENCE(S) - PROCECO project supported by Ville de Paris. We are grateful to the INRAE MIGALE bioinformatics facility (MIGALE, INRAE, 2020. Migale bioinformatics Facility, doi: 10.15454/1.5572390655343293E12) for providing computing resources.

## A Contrasts

In this section, we give some details about the calculations of the contrasts for both the Poisson and the marked Poisson models given in Sections 4 and 5 respectively.

**Least-squares Poisson contrast.** The least-squares criterion of a given path  $N$  and for a fixed  $\nu \in \Upsilon_\star^{K,n}$  and any  $\tau \in \mathcal{P}_\nu^K(N)$  is

$$LS_P(N; \tau, \lambda) = \sum_{k=1}^K (\Delta\tau_k \lambda_k^2 - \Delta N_k \lambda_k), \quad (23)$$

that is minimal for the same intensities  $\hat{\lambda}_k(\tau) = \frac{\Delta N_k}{\Delta\tau_k}$ ,  $1 \leq k \leq K$ . The associated contrast function of  $\tau$  is therefore as follows

$$\tilde{\gamma}_P(\tau) = LS_P(N; \tau, \hat{\lambda}) = - \sum_{k=1}^K \frac{\nu_k}{\Delta\tau_k} = \sum_{k=1}^K C(\nu_k, \Delta\tau_k). \quad (24)$$

Similarly to the likelihood contrast, it is straightforward to see that both assumptions 3.1 and 3.2 are satisfied. Moreover, it shares the same undesirable property: for  $K > 2$ , the optimal segmentation inevitably contains segments of null length.

**Poisson-Gamma based-likelihood contrast.** Recall that the intensities  $\lambda_k$  are assumed to be independent random variables and follow a gamma distribution with parameters  $a > 0$  and  $b > 0$ , denoted  $\mathcal{G}\text{amma}(a, b)$ . The distribution of  $\lambda$  is thus

$$p_G(\lambda; a, b) = \prod_{k=1}^K \frac{b^a}{\Gamma(a)} \lambda_k^{(a-1)} e^{-b\lambda_k},$$

where  $\Gamma$  represents for the gamma function:  $\Gamma(a) = \int_0^{+\infty} e^{-t} t^{a-1} dt$ . For a given  $\tau$ , the joint distribution of  $(N, \lambda)$  is therefore

$$p_{PG}(N, \lambda; \tau, a, b) = p_P(N; \lambda, \tau) p_G(\lambda; a, b) = \prod_{k=1}^K \frac{b^a}{\Gamma(a)} \lambda_k^{(\Delta N_k + a - 1)} e^{-(\Delta\tau_k + b)\lambda_k},$$

and the marginal distribution of  $N$  is

$$p_{PG}(N; \tau, a, b) = \int p_{PG}(N, \lambda; \tau, a, b) d\lambda = \prod_{k=1}^K \frac{b^a \Gamma(\Delta N_k + a)}{\Gamma(a) (\Delta\tau_k + b)^{\Delta N_k + a}}.$$

For a fixed  $\nu \in \Upsilon_\star^{K,n}$  and all  $\tau \in \mathcal{P}_\nu^K(N)$ , the proposed contrast, the so-called Poisson-Gamma contrast, is then

$$\gamma_{PG}(\tau) = -\log p_{PG}(N | \tau; a, b) = \sum_{k=1}^K \left( -a \log b + \log \Gamma(a) + \tilde{a}_k \log \tilde{b}_k - \log \Gamma(\tilde{a}_k) \right),$$

where  $\tilde{a}_k = \nu_k + a$ ,  $\tilde{b}_k = \Delta\tau_k + b$ .

**Marked Poisson-Gamma-Exponential-Gamma based-likelihood contrast.** Recall that the  $\lambda_k$ 's and  $\rho_k$ 's are assumed to be independent random variables and follow a Gamma distribution with parameters  $a_\lambda > 0$  and  $b_\lambda > 0$  and a Gamma distribution with parameters  $a_\rho > 0$  and  $b_\rho > 0$ , respectively. For a given  $\boldsymbol{\tau}$ , the joint distribution of  $(N, X, \boldsymbol{\lambda}, \boldsymbol{\rho})$  is thus

$$\begin{aligned} p_{MPGEG}(N, X, \boldsymbol{\lambda}, \boldsymbol{\rho}; \boldsymbol{\tau}, a_\lambda, b_\lambda, a_\rho, b_\rho) &= p_P(N, X; \boldsymbol{\tau}, \boldsymbol{\lambda}, \boldsymbol{\rho}) p_G(\boldsymbol{\lambda}; a_\lambda, b_\lambda) p_G(\boldsymbol{\rho}; a_\rho, b_\rho), \\ &= \prod_{k=1}^K \frac{b_\lambda^{a_\lambda}}{\Gamma(a_\lambda)} \lambda_k^{(\Delta N_k + a_\lambda - 1)} e^{-(\Delta \tau_k + b_\lambda) \lambda_k} \\ &\quad \times \prod_{k=1}^K \frac{b_\rho^{a_\rho}}{\Gamma(a_\rho)} \rho_k^{(\Delta N_k + a_\rho - 1)} e^{-(S_k + b_\rho) \rho_k}, \end{aligned}$$

and the marginal distribution of  $(N, X)$  is

$$\begin{aligned} p_{MPGEG}(N, X; \boldsymbol{\tau}, a_\lambda, b_\lambda, a_\rho, b_\rho) &= \iint p_{PGEG}(N, \boldsymbol{\lambda}, \boldsymbol{\rho}; \boldsymbol{\tau}, a_\lambda, b_\lambda, a_\rho, b_\rho) d\boldsymbol{\lambda} d\boldsymbol{\rho}, \\ &= \prod_{k=1}^K \frac{b_\lambda^{a_\lambda} \Gamma(\Delta N_k + a_\lambda)}{\Gamma(a_\lambda) (\Delta \tau_k + b_\lambda)^{\Delta N_k + a_\lambda}} \frac{b_\rho^{a_\rho} \Gamma(\Delta N_k + a_\rho)}{\Gamma(a_\rho) (S_k + b_\rho)^{\Delta N_k + a_\rho}}. \end{aligned}$$

For a fixed  $\boldsymbol{\nu} \in \Upsilon_\star^{K,n}$  and for any  $\boldsymbol{\tau} \in \mathcal{P}_\nu^K(N)$ , the MPGEG contrast is then

$$\begin{aligned} \gamma_{MPGEG}(\boldsymbol{\tau}) &= -\log p_{MPGEG}(N; \boldsymbol{\tau}, a_\lambda, b_\lambda, a_\rho, b_\rho), \\ &= \sum_{k=1}^K \left( \tilde{a}_{k,\lambda} \log \tilde{b}_{k,\lambda} - \log \Gamma(\tilde{a}_{k,\lambda}) \right) + \left( \tilde{a}_{k,\rho} \log \tilde{b}_{k,\rho} - \log \Gamma(\tilde{a}_{k,\rho}) \right) \\ &\quad + K \left( -a_\lambda \log b_\lambda + \log \Gamma(a_\lambda) - a_\rho \log b_\rho + \log \Gamma(a_\rho) \right), \end{aligned}$$

where  $\tilde{a}_{k,\lambda} = \nu_k + a_\lambda$ ,  $\tilde{b}_{k,\lambda} = \Delta \tau_k + b_\lambda$ ,  $\tilde{a}_{k,\rho} = \nu_k + a_\rho$ , and  $\tilde{b}_{k,\rho} = S_k + b_\rho$ .

## B Dynamic Programming (DP) algorithm

In this section, we describe the principle of the standard Dynamic Programming algorithm for a discrete segmentation problem and specify how to apply it on a finite and given grid as in our case.

**DP for discrete change-points problem.** If we observed an ordered sequence of  $A$  observations, the goal is to find a partition of the discrete grid  $\llbracket 1, A \rrbracket$  into  $K$  segments delimited by  $K - 1$  change-points denoted  $a_k$  for  $k = 1, \dots, K - 1$  with the convention  $a_0 = 0$  and  $a_K = A$ . The  $k$ -th segment is  $\llbracket a_{k-1} + 1, a_k \rrbracket$  and we define the set of all possible segmentations with  $K - 1$  change-points:

$$\mathcal{A}_A^K = \{ \mathbf{a} = (a_1, a_2, \dots, a_{K-1}) \in \mathbb{N}^{K-1} : a_0 = 0 < a_1 < \dots < a_{K-1} < a_K = A \},$$

with cardinality  $\binom{A-1}{K-1}$ . Even though this space is finite, it is extremely large and a naive search is computationally prohibitive. The well-known solution consists of using the DP algorithm which can be applied if and only if the quantity to be optimized is segment-additive:

$$\hat{\mathbf{a}} = (\hat{a}_1, \hat{a}_2, \dots, \hat{a}_{K-1}) = \underset{\mathbf{a} \in \mathcal{A}_A^K}{\operatorname{argmin}} R_{\mathbf{a}} = \underset{\mathbf{a} \in \mathcal{A}_A^K}{\operatorname{argmin}} \sum_{k=1}^K C(a_{k-1} + 1 : a_k),$$

where  $R_{\mathbf{a}}$  is called the cost of the segmentation  $\mathbf{a}$  and  $C(a_{k-1} + 1 : a_k) = C(\llbracket a_{k-1} + 1, a_k \rrbracket)$  the cost of the segment  $\llbracket a_{k-1} + 1, a_k \rrbracket$ . We define

$$C_{K,A} = \min_{\mathbf{a} \in \mathcal{A}_A^K} \sum_{k=1}^K C(a_{k-1} + 1 : a_k),$$

the cost of the best segmentation in  $K$  segments. If we note  $C(i : j) = C(\llbracket i, j \rrbracket)$  the cost of the segment  $\llbracket i, j \rrbracket$ , thanks to the segment-additivity property of  $R_{\mathbf{a}}$ , DP solves the optimization problem using the following update rule:

$$C_{K,A} = \min_{0 < a_1 < \dots < a_{K-1} < A} \sum_{k=1}^K C(a_{k-1} + 1 : a_k) = \min_{K-1 \leq h < A} \{C_{K-1,h} + C(h + 1 : A)\}.$$

This algorithm requires calculating the cost of each possible segment which is

$$\begin{aligned} C(i : j) &= C(\llbracket i, j \rrbracket) \quad \text{if } 1 \leq i \leq j \leq A \\ &= +\infty \quad \text{otherwise.} \end{aligned}$$

**Search in a fixed and finite grid.** Let

$$\mathbf{tp} = \{\text{tp}_1, \text{tp}_2, \dots, \text{tp}_A\},$$

be this grid where  $0 < \text{tp}_i < 1$  and  $A$  is the size of the grid or the number of potential change-points. If a segment is defined as  $(\text{tp}_\ell, \text{tp}_h]$  with  $\ell < h$ , we can apply DP with

$$\begin{aligned} C(i : j) &= C((\text{tp}_{i-1}, \text{tp}_j]) \quad \text{if } 1 \leq i \leq j \leq A + 1 \\ &= +\infty \quad \text{otherwise.} \end{aligned}$$

with the convention  $\text{tp}_0 = 0$  and  $\text{tp}_{A+1} = 1$ . The complexity is thus  $\mathcal{O}((A + 1)^2 K)$  and the optimal change-points are given by

$$\hat{\tau}_k = \text{tp}_{\hat{a}_k}.$$

## C Simulation parameters

We provide here measures of the difficulty of the segmentation problems considered in the simulation study presented in Section 8. To this aim, we define a signal-to-noise ratio (SNR) measure as

$$\text{SNR} = \sqrt{\frac{\Delta\tau_- \lambda_-^2 + \Delta\tau_+ \lambda_+^2 - \bar{\lambda}^2}{\bar{\lambda}}} \quad (25)$$

This definition of the SNR is consistent with this used in the Gaussian setting to measure the difficulty of a segmentation problem (see e.g. Picard et al., 2011). The SNR is zero when the intensity  $\lambda$  is constant. Table 2 gives the values of  $\lambda_-$  and  $\lambda_+$  for each combination  $(\bar{\lambda}, \lambda_R)$  considered in the simulation design described in Section 8.1. Table 3 gives the corresponding SNR values.

To make the SNR measure even more interpretable, we relate it to the power of the Kolmogorov-Smirnoff (KS) for the uniform distribution of the event times over  $(0, 1)$ . In absence of signal (constant intensity  $\lambda$ ), the events are uniformly distributed over  $(0, 1)$ . When the segmentation structure gets stronger (higher SNR), the KS is more and more capable of detecting a departure from the uniform

Table 2: Values of  $\lambda_-$ ,  $\lambda_+$  for each combination  $\bar{\lambda}/\lambda_R$  used in the simulation study. The case  $\lambda_R = 1$  ( $\lambda_- = \lambda_+ = \bar{\lambda}$ ) is not displayed.

$\bar{\lambda}$	$\lambda_R$						
	2	3	4	6	8	11	16
32	25–50	20–60	17–68	13–78	11–88	8–88	6–96
56	43–86	35–105	30–120	23–138	18–144	14–154	10–160
100	77–154	63–189	53–212	41–246	33–264	26–286	19–304
178	138–276	112–336	95–380	72–432	59–472	45–495	33–528
316	245–490	200–600	169–676	129–774	104–832	81–891	59–944
562	435–870	355–1065	300–1200	229–1374	185–1480	143–1573	105–1680
1000	774–1548	632–1896	533–2132	407–2442	329–2632	255–2805	186–2976

Table 3: Values of  $SNR$  for the different values of  $\bar{\lambda}$  and  $\lambda_R$  used in the simulation study.

$\bar{\lambda}$	$\lambda_R$						
	2	3	4	6	8	11	16
32	2.15	3.11	4.07	5.21	6.42	6.32	7.27
56	2.43	4.11	5.51	7.06	7.49	8.37	8.87
100	3.34	5.68	7.14	9.40	10.54	11.97	13.12
178	4.75	7.54	9.72	12.18	14.17	15.22	16.83
316	6.34	10.29	13.03	16.56	18.63	20.77	22.68
562	8.33	13.62	17.28	22.00	24.86	27.35	30.28
1000	11.10	18.20	22.96	29.27	33.12	36.62	40.10

distribution.

Figure 14 shows how the power of the KS increases as the SNR increases. We observe that for SNR smaller than 10 (see Table 3), the power of the KS test is low, meaning simply detecting heterogeneity is a difficult task. Note that detecting heterogeneity is a much simpler task than precisely locating change-points and estimating the intensity between each of them. We see that the configurations considered in the proposed simulation designed range from very difficult (very low power of the KS test) to fairly easy.

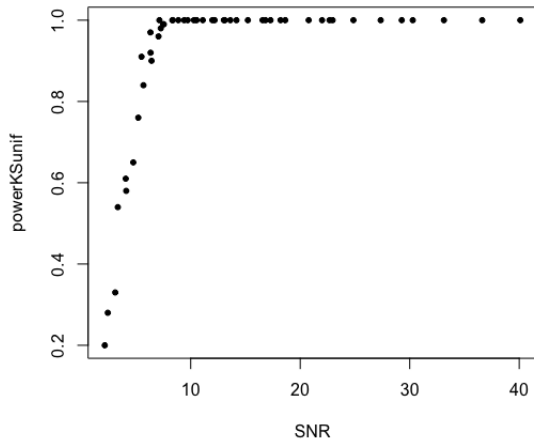


Figure 14: Power of the Kolmogorov-Smirnov (KS) for the uniform distribution of the event times, as a function of the SNR. Each dot corresponds to a given combination  $(\bar{\lambda}, \lambda_R)$  used in the simulation.

## D Simulation of PHP

We present here an algorithm for sampling from the presented PHP. The algorithm we employ is the modified thinning algorithm proposed by Ogata (1981) for sampling from an HP process (see also Daley and Vere-Jones, 2006; Rasmussen, 2018; Laub et al., 2021).

Consider a PHP with conditional intensity function  $\lambda(t)$ . Conceptually, the thinning algorithm we use to sample from  $N$  in  $[0, T]$  resembles an accept/reject mechanism: initially generating more points than required in  $[0, T]$  using a larger intensity than  $\lambda$ . In other words, points are sampled according to a Poisson process of intensity function  $M(t)$  satisfying  $M(t) > \lambda(t)$  for all  $t \in [0, T]$ . Subsequently, some of these points are discarded with a certain probability, ensuring that the retained points follow the desired distribution. Precisely, each point is deleted with a probability  $1 - \lambda/M$ . The retained points form a sample from a point process of conditional intensity  $\lambda(t)$ ; see (Ogata, 1981, Proposition 1).



---

**Algorithm 2** Sampling from a point process of conditional intensity  $\lambda$  and history  $H_t$ 

---

```
1: input conditional intensity  $\lambda$ 
2: set  $t=0, i=0$ 
3: while  $t \leq T$  do
4:   compute  $M(t)$  via Equation (26)
5:   generate independent r.v.  $s \sim \text{Exp}(1/M(t))$  and  $u \sim \text{Unif}(0, 1)$ 
6:   set  $p = \lambda(t + s \mid H_{t+s})/M(t)$  the retaining probability of the proposed point  $t + s$ 
7:   if  $t + s < T$  and  $u \leq p$  then
8:     update  $i = i + 1$ 
9:     set  $t_i = t + s$  (accept the proposed point)
10:  end if
11:  update  $t = t + s$ 
12: end while
13: return  $\{t_i\}_i$ 
```

---

Note that the selection of the function  $M$  plays a crucial role in the simulation process. On one hand,  $M$  should satisfy  $M(t) > \lambda(t)$  for all  $t \in [0, T]$  ensuring that the intensity of proposed points exceeds the conditional intensity of the PHP. On the other hand,  $M$  need to be close to  $\lambda$  to maximize the simulation's efficiency, thereby minimizing the number of rejected points. Following Ogata (1981), we opt for the function  $M$  defined for  $t \in [0, T]$  by

$$M(t) := \lambda(t) + \alpha \sum_{k=1}^K c_k \mathbb{1}_{[\tau_{k-1}, \tau_k)}(t). \quad (26)$$

## E Additional simulations

This section is dedicated to the study of the robustness of the proposed method to the two tuning parameters that are,

- the hyper-parameters  $(a, b)$  used in the Poisson-Gamma contrast defined in Equation (11) and
- the sampling fraction  $f$  for the cross-validation procedure described in Section 7.

For both parameters, we use the simulation design described in Section 8.1, with the two typical parameters  $\bar{\lambda} = 100$  and  $\lambda_R = 8$ . These values are chosen, as they yield in average performances for the proposed algorithm, as shown in Figures 3 and 4.

**Hyper-parameters of the Poisson-Gamma contrast.** Regarding the choice of the  $(a, b)$ , we stick to the rule  $a/b = n$ , which guarantees that the expectation of  $N(T)$  is  $n$ . Hence, we are left with the choice of  $a = nb$ , reminding that the variance of the Gamma distribution  $\mathcal{Gamma}(a, b)$  is  $a/b^2$ , which increases as  $a$  decreases (as  $b = a/n$ ). We consider five values for  $a$ :  $a = 0.1, 0.5, 1, 2$  and  $10$ .

Figure 15 (left) shows that the averaged selected  $\hat{K}$  is close to the true one ( $K = 6$ ) for all values of  $a$  and that the suggested value  $a = 1$  yields the lower variance. The center panel of the same figure shows that the best precision for the change-point locations, measured by the Hausdorff distance  $d(\hat{\tau}, \tau)$ , is obtained for  $a = 1$  or  $2$ . Finally, the right panel, shows that the relative  $L^2$  distance between the estimated and true cumulated intensity is fairly insensitive to the choice of  $a$ . Overall, this suggests that the recommendation  $(a = 1, b = 1/n)$  is a reasonable and simple choice for the hyper-parameters.

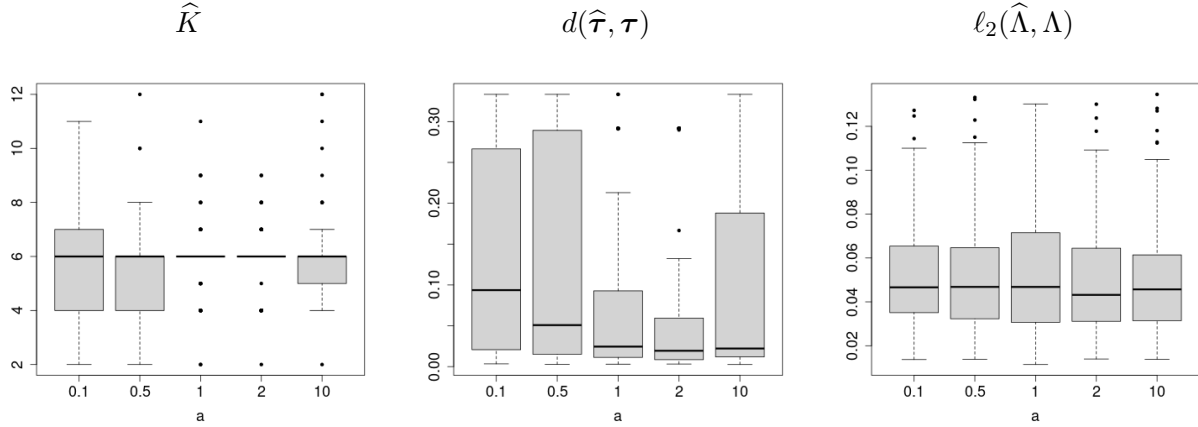


Figure 15: Effect of the choice of the hyper-parameter  $a$  on three evaluation criteria for  $\bar{\lambda} = 100$ ,  $\lambda_R = 8$  and for a true number of segments  $K = 6$ . Left: selected number of segments  $\hat{K}$  using cross-validation; Center: Hausdorff distance between the estimated change-points  $\hat{\tau}$  and the true ones  $\tau$ ; Right: relative  $L^2$ -norm between the estimated and the true cumulated intensity functions.

**Sampling fraction for cross-validation.** In the simulation study presented in Section 8, a fraction  $f = 4/5$  of the data is used to build each learning set. We consider here the fractions  $f = 1/2, 2/3, 4/5$  and  $9/10$ .

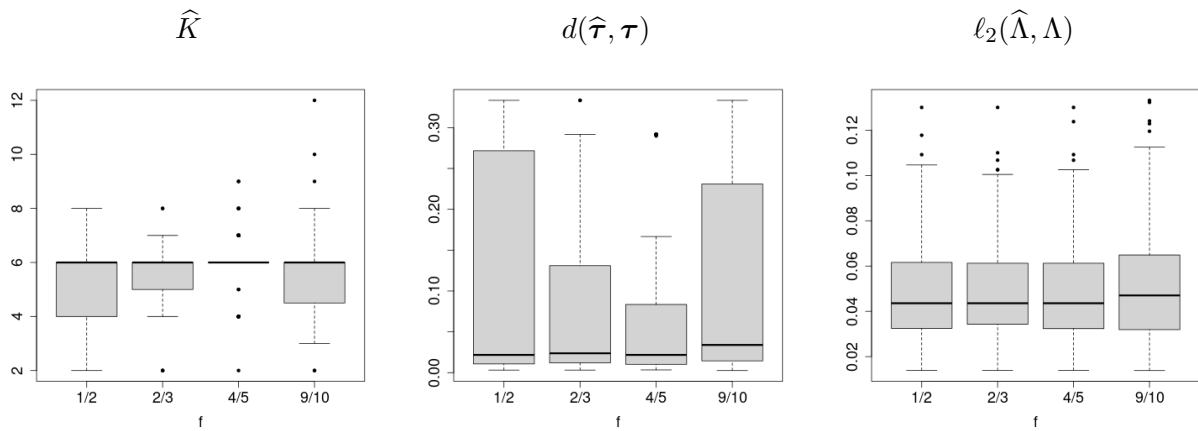


Figure 16: Effect of the choice of the fraction  $f$  used in the cross-validation procedure described in Section 7 on three evaluation criteria for  $\bar{\lambda} = 100$ ,  $\lambda_R = 8$  and for a true number of segments  $K = 6$ . Left, center and right: same legend as Figure 15.

Figure 16 (left) shows that all values of  $f$  give the right number of segment  $K$  in average, but that the recommended value  $f = 4/5$  yields the smallest variance. It also yields the smallest Hausdorff distance between the estimated and true change-points (center), while the relative  $L^2$  distance between the estimate  $\hat{\Lambda}$  and the true  $\Lambda$  is unaffected by the choice of  $f$ . The fraction  $f = 4/5$  therefore seems to be a reasonable choice for the cross-validation in our case.

## F Read life data sets illustrations

Figure 17 displays the segmentations of the Mauna Loa series obtained by considering  $K = 3, 4, 5$  and 6 segments. The fit obviously improves as  $K$  increases and the cross-validation procedure proposed in Section 7 aims to avoid overfitting. Exploring higher values of  $K$  may still be useful for uncovering tiny heterogeneity, which might merit further investigation (see, e.g., the 1870-1880 segment exhibited with  $K = 6$ ).

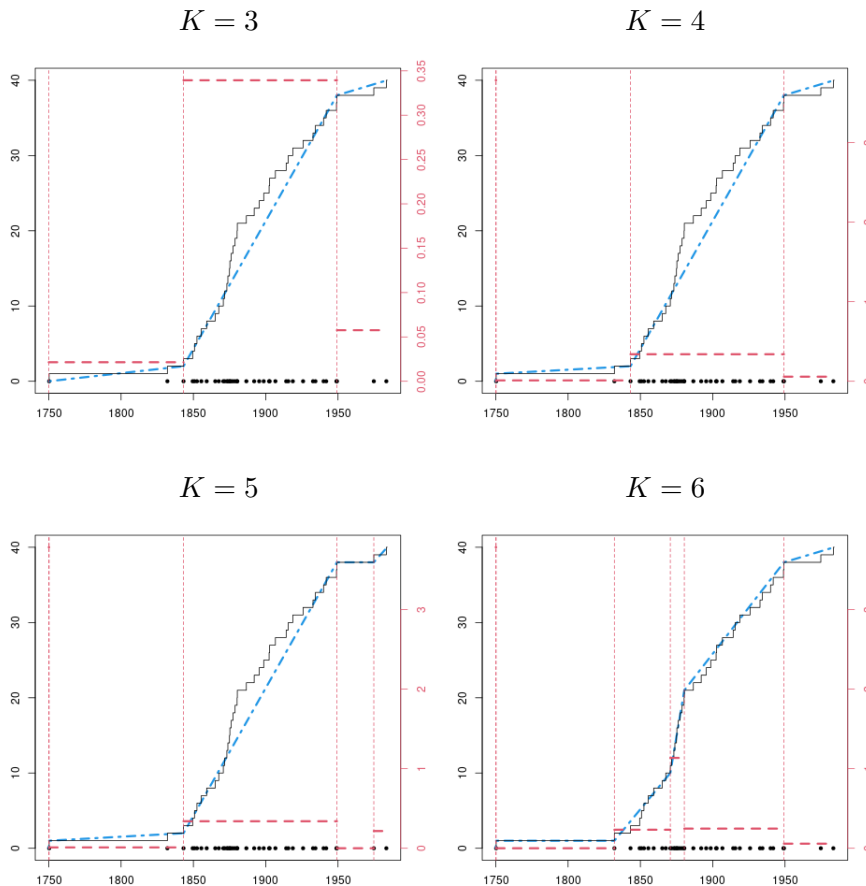


Figure 17: Eruptions of the Mauna Loa volcano. Segmentation with  $K = 3, 4, 5, 6$  segments. Same legend as Figure 9. Note that the scale of the right  $y$ -axis differs between plots. The first segment for  $K = 4, 5$  and 6 is included in the first year of observation (1750) and contains only one event.

## References

- J. Achcar, E. Martinez, A. Ruffino-Netto, C. Paulino, and P. Soares. A statistical model investigating the prevalence of tuberculosis in new york city using counting processes with two change-points. *Epidemiology & Infection*, 136(12):1599–1605, 2008.
- J. A. Achcar, E. R. Rodrigues, and G. Tzintzun. Using non-homogeneous poisson models with multiple change-points to estimate the number of ozone exceedances in mexico city. *Environmetrics*, 22(1): 1–12, 2011.

- P. K. Andersen, Ø. Borgan, R. D. Gill, and N. Keiding. *Statistical models based on counting processes*. Springer Series in Statistics. Springer-Verlag, New York, 1993.
- S. Arlot and A. Celisse. Segmentation of the mean of heteroscedastic data via cross-validation. *Statistics and Computing*, 21(4):613–632, 2011.
- I. E. Auger and C. E. Lawrence. Algorithms for the optimal identification of segment neighborhoods. *Bull. Math. Biol.*, 51(1):39–54, 1989.
- J. Bai and P. Perron. Computation and analysis of multiple structural change models. *Journal of applied econometrics*, 18(1):1–22, 2003.
- M. S. Bebbington. Identifying volcanic regimes using hidden markov models. *Geophysical Journal International*, 171(2):921–942, 2007.
- Y. Bessy-Roland, A. Boumezoued, and C. Hillairet. Multivariate hawkes process for cyber insurance. *Annals of Actuarial Science*, 15(1):14–39, 2021.
- S. Chakar, E. Lebarbier, C. Lévy-Leduc, S. Robin, et al. A robust approach for estimating change-points in the mean of an AR(1) process. *Bernoulli*, 23(2):1408–1447, 2017.
- A. Cleynen and E. Lebarbier. Model selection for the segmentation of multiparameter exponential family distributions. *Electronic Journal of Statistics*, 11(1):800–842, 2017.
- D. Daley and D. Vere-Jones. *An Introduction to the Theory of Point Processes: Volume I: Elementary Theory and Methods*. Probability and Its Applications. Springer New York, 2006. ISBN 9780387215648.
- D. Daley and D. Vere-Jones. *An introduction to the theory of point processes: volume II: general theory and structure*. Springer Science & Business Media, 2007.
- D. J. Daley and D. Vere-Jones. *An introduction to the theory of point processes: volume II: general theory and structure*. Springer, 2008.
- N. El Karoui, S. Loisel, and Y. Salhi. Minimax optimality in robust detection of a disorder time in doubly-stochastic poisson processes. *The Annals of Applied Probability*, 27(4):2515–2538, 2017.
- M. Fromont, F. Grela, and R. Le Guével. Minimax and adaptive tests for detecting abrupt and possibly transitory changes in a poisson process. *Electronic Journal of Statistics*, 17(2):2575–2744, 2023.
- A. Gupta and J. Baker. A bayesian change point model to detect changes in event occurrence rates, with application to induced seismicity. In *12th International Conference on Applications of Statistics and Probability in Civil Engineering*, pages 12–15. The Univ. of British Columbia Vancouver, Canada, 2015.
- D. Harte. Ptprocess: An r package for modelling marked point processes indexed by time. *Journal of Statistical Software*, 35:1–32, 2010.
- C.-H. Ho and M. Bhaduri. A quantitative insight into the dependence dynamics of the Kilauea and Mauna Loa volcanoes, Hawaii. *Mathematical Geosciences*, 49(7):893–911, 2017.
- B. Jackson, J. D. Scargle, D. Barnes, S. Arabhi, A. Alt, P. Gioumoussis, E. Gwin, P. Sangtrakulcharoen, L. Tan, and T. T. Tsai. An algorithm for optimal partitioning of data on an interval. *Signal Processing Letters, IEEE*, 12(2):105–108, 2005.

- R. Killick, P. Fearnhead, and I. A. Eckley. Optimal detection of changepoints with a linear computational cost. *Journal of The American Statistical Association*, 107(500):1590–1598, 2012.
- P. J. Laub, Y. Lee, and T. Taimre. *The elements of Hawkes processes*. Springer, 2021.
- M. Lavielle. Using penalized contrasts for the change-point problem. *Signal Processing*, 85(8):1501–1510, 2005.
- E. Lebarbier. Detecting multiple change-points in the mean of gaussian process by model selection. *Signal processing*, 85(4):717–736, 2005.
- S. Li, Y. Xie, M. Farajtabar, A. Verma, and L. Song. Detecting changes in dynamic events over networks. *IEEE Transactions on Signal and Information Processing over Networks*, 3(2):346–359, 2017a.
- S. Li, Y. Xie, M. Farajtabar, A. Verma, and L. Song. Detecting changes in dynamic events over networks. *IEEE Transactions on Signal and Information Processing over Networks*, 3(2):346–359, 2017b.
- Y. S. Niu, N. Hao, and H. Zhang. Multiple change-point detection: a selective overview. *Statistical Science*, 31(4):611–623, 2016.
- Y. Ogata. On lewis’ simulation method for point processes. *IEEE Transactions on Information Theory*, 27(1):23–31, 1981. doi: 10.1109/TIT.1981.1056305.
- F. Papangelou. Integrability of expected increments of point processes and a related random change of scale. *Transactions of the American Mathematical Society*, 165:483–506, 1972.
- L. Passarelli, B. Sansò, L. Sandri, and W. Marzocchi. Testing forecasts of a new bayesian time-predictable model of eruption occurrence. *Journal of volcanology and geothermal research*, 198(1-2): 57–75, 2010.
- F. Picard, E. Lebarbier, M. Hoebeke, G. Rigaiil, B. Thiam, and S. Robin. Joint segmentation, calling, and normalization of multiple cgh profiles. *Biostatistics*, 12(3):413–28, 2011.
- A. Raftery and V. Akman. Bayesian analysis of a poisson process with a change-point. *Biometrika*, 73(1):85–89, 1986.
- J. G. Rasmussen. Lecture notes: Temporal point processes and the conditional intensity function, 2018.
- L. Shaochuan. Bayesian multiple changepoint detection for stochastic models in continuous time. *Bayesian Analysis*, 16(2):521–544, 2021.
- J. J. Shen and N. R. Zhang. Change-point model on nonhomogeneous poisson processes with application in copy number profiling by next-generation dna sequencing. *The Annals of Applied Statistics*, 6(2):476–496, 2012.
- G. Shmueli and H. Burkom. Statistical challenges facing early outbreak detection in biosurveillance. *Technometrics*, 52(1):39–51, 2010.
- S. Spaziani, G. Girardeau, I. Bethus, and P. Reynaud-Bouret. Heterogeneous multiscale multivariate autoregressive model: Existence, sparse estimation and application to functional connectivity in neuroscience. *Annals of Statistics*, 2023.

- J.-C. Tanguy, M. Condomines, M. Le Goff, V. Chillemi, S. La Delfa, and G. Patanè. Mount etna eruptions of the last 2,750 years: revised chronology and location through archeomagnetic and 226 ra-230 th dating. *Bulletin of Volcanology*, 70:55–83, 2007.
- C. Truong, L. Oudre, and N. Vayatis. Selective review of offline change point detection methods. *Signal Processing*, 167:107299, 2020.
- K.-L. Tsui, W. Chiu, P. Gierlich, D. Goldsman, X. Liu, and T. Maschek. A review of healthcare, public health, and syndromic surveillance. *Quality Engineering*, 20(4):435–450, 2008.
- H. Wang, L. Xie, Y. Xie, A. Cuzzo, and S. Mak. Sequential change-point detection for mutually exciting point processes. *Technometrics*, 65(1):44–56, 2023.
- W. R. West and T. R. Ogden. Continuous-time estimation of a change-point in a poisson process. *Journal of Statistical Computation and Simulation*, 56(4):293–302, 1997.
- T. Young Yang and L. Kuo. Bayesian binary segmentation procedure for a poisson process with multiple changepoints. *Journal of Computational and Graphical Statistics*, 10(4):772–785, 2001.
- N. R. Zhang and D. O. Siegmund. A modified Bayes information criterion with applications to the analysis of comparative genomic hybridization data. *Biometrics*, 63(1):22–32, 2007.